Space Sci Rev
DOI 10.1007/s11214-014-0080-4

Science Enhancements by the MAVEN Participating Scientists

J. Grebowsky · K. Fast · E. Talaat · M. Combi · F. Crary · S. England · Y. Ma · M. Mendillo · P. Rosenblatt · K. Seki · M. Stevens · P. Withers

Received: 18 February 2014 / Accepted: 8 July 2014

Abstract NASA implemented a Participating Scientist Program and released a solicitation for the Mars Atmosphere and Volatile EvolutioN mission (MAVEN) proposals on February 14, 2013. After a NASA peer review panel evaluated the proposals, NASA Headquarters selected nine on June 12, 2013. The program's intent is to enhance the science return from the mission by including new investigations that broaden and/or complement the base-

J. Grebowsky (✉)
NASA Goddard Space Flight Center, Greenbelt, MD 20771, USA
e-mail: joseph.m.grebowsky@nasa.gov

K. Fast · E. Talaat
NASA Headquarters, Washington, DC 20546, USA

M. Combi
University Michigan, Ann Arbor, MI 48109, USA

F. Crary
University Colorado, Boulder, CO 80303, USA

S. England
Space Sciences Laboratory, University of California Berkeley, Berkeley, CA 94720, USA

Y. Ma
University of California, Los Angeles, CA 90095, USA

M. Mendillo · P. Withers
Boston University, Boston, MA 02215, USA

P. Rosenblatt
Royal Observatory of Belgium, Brussels, Belgium

K. Seki
Nagoya University, Nagoya 464-8601, Japan

M. Stevens
Space Science Division, Naval Research Laboratory, Washington, DC 203751, USA

Published online: 02 September 2014

line investigations, while still addressing key science goals. The selections cover a broad range of science investigations. Included are: a patching of a 3D exosphere model to an improved global ionosphere-thermosphere model to study the generation of the exosphere and calculate the escape rates; the addition of a focused study of upper atmosphere variability and waves; improvement of a multi-fluid magnetohydrodynamic model that will be adjusted according to MAVEN observations to enhance the understanding of the solar-wind plasma interaction; a global study of the state of the ionosphere; folding MAVEN measurements into the Mars International Reference Ionosphere under development; quantification of atmospheric loss by pick-up using ion cyclotron wave observations; the reconciliation of remote and in situ observations of the upper atmosphere; the application of precise orbit determination of the spacecraft to measure upper atmospheric density and in conjunction with other Mars missions improve the static gravity field model of Mars; and an integrated ion/neutral study of ionospheric flows and resultant heavy ion escape. Descriptions of each of these investigations are given showing how each adds to and fits seamlessly into MAVEN mission science design.

Keywords Mars · Aeronomy · Thermosphere · Ionosphere magnetosphere MAVEN mission

1 Background

1.1 Motivation for the Enhancement of MAVEN's Science Team

NASA science missions are planned with specific science goals, and the spacecraft, science team, and science operations are designed to that end. In order to augment expertise, bring fresh perspective and reap the benefit of additional insights and ideas while the mission can actively respond to them, NASA may employ a mission Participating Scientist Program. Participating scientists augment the scientific return from a mission by broadening involvement by researchers from outside the already established science team. Participating scientists augment the existing science team to include new investigations that enhance and/or complement the currently funded investigations to advance the state of knowledge. A Participating Scientist Program may also invite international participation through selected high-impact investigations by non-US scientists without US financial support.

The objectives of the MAVEN Participating Scientist Program are to enhance the scientific return from the mission by augmenting the existing science team to include new Mars science investigations that enhance and/or supplement the funded Principal Investigator (PI)-led investigations, thus maximizing the contribution of the mission to the future exploration and scientific understanding of Mars. The second and equally important goal of this opportunity is to increase the number of scientists supporting daily mission operations and aiding in mission planning and data archiving. The program saw many applicants, including a number from outside of the US, and the proposed investigations underwent a competitive review by experts from the scientific community. These participating scientists selected through this process bring investigations that complement the MAVEN mission's science questions in a manner that does not duplicate planned science investigations, and they will also support mission planning and execution. They have become members of the science team and their participation in the real-time response to new observations will enable their science investigations and enhance the overall science return from MAVEN.

Table 1 Listing of MAVEN Participating Scientist awards

Participating scientist principal investigator	Institution	Maven Studies
Pascal Rosenblatt	Royal Observatory of Belgium	Radio Science Investigations
Scott England	U. California, Berkeley	Mars Upper Atmosphere Variability and Connection to Lower Atmosphere
Michael Stevens	Naval Research Laboratory	Upper Atmosphere: Reconciling Remote Observations with In situ Measurements
Paul Withers	Boston University	Integration of Neutral and Plasma Observations
Michael Mendillo	Boston University	Semi-Empirical Modeling of Martian Ionosphere and its Day-To-Day Variability
Michael Combi	U. Michigan	Distributions and Escape Rates of Atomic Neutrals from the Upper Atmosphere of Mars
Kanako Seki	Nagoya University	Effects of Regional Couplings on Atmospheric Flows and the Atmospheric Escape from Mars
Yingjuan Ma	University of California, Los Angeles	MHD Study of the Solar Wind Induced Plasma Escape from Martian Atmosphere
Frank Crary	U. Colorado, Boulder	Multi-Instrument Study of Ionospheric Loss from Mars

1.2 The Added Science

The Participating Scientist proposals received and accepted typically addressed one or more of MAVEN's three key Mars science questions:

1. *What is the current state of the upper atmosphere and what processes control it?*
   This involves spatial and temporal characterization of the key components of the upper atmosphere—which includes the ionized components.
2. *What is the escape rate at the present epoch and how does it relate to the controlling processes?*
   This involves measurements and modeling of escape rates and processes in response to variations in measured solar energy inputs.
3. *What has the total loss to space been through time?*
   Using main sequence stellar observations to define the evolution of the Sun's historical energy output through time, the variations of the upper atmosphere system and losses at the current epoch in response to solar activity changes provides the information needed to extrapolate the history of Mars' volatile escape into the past.

The proposals were peer reviewed and nine were selected by NASA, two from non-USA institutions. The accepted proposals utilize the entire range of MAVEN's broad scope of measurement capabilities, from the lower atmosphere to the solar wind, and add significant contributions to the exploration of the key processes that couple the solar energy inputs to atmospheric escape. The accepted task titles (and the Participating Scientist teams' Principal Investigators), in rough order of the altitudes of their prime interest, from low to high, are listed in Table 1. Figure 1 sketches how the Participating Scientist realms of investigations extend through all the spatial regions that the MAVEN spacecraft is going to traverse.

The Rosenblatt study will measure, through precise radio tracking of the spacecraft orbit, low altitude atmosphere density variations and improve our understanding of the Mars

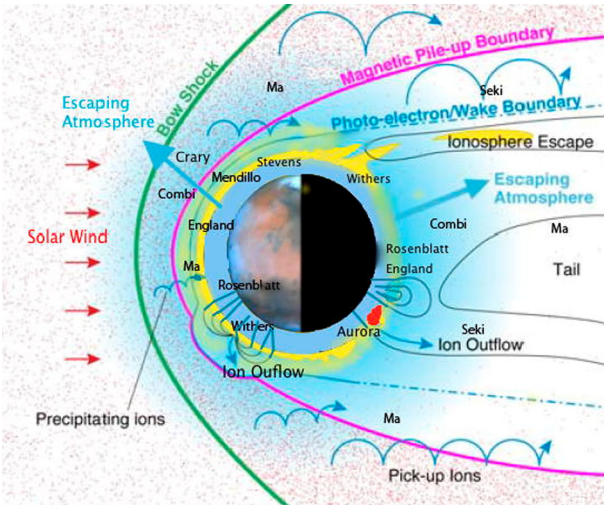

Fig. 1 Rough sketch of regions where the Participating Scientists (identified by the individual leads of each investigation) will make contributions to the science of MAVEN. The ensemble of studies encompasses all regions to be covered by MAVEN

Gravity field. The England task will look further into the upper atmosphere variability by using in situ and remote sensing MAVEN observations to bracket atmospheric wave and climate variability. Using the same instruments, Stevens' Participating Scientist objective is to synoptically quantify global-scale compositional variability in the upper atmosphere of Mars.

Although the neutral atmosphere is the parent of all escaping species to be explored by MAVEN, the ionosphere is one of its progenies that plays a very significant role in atmospheric escape. In this ionized regime of the upper atmosphere the Withers and Mendillo efforts will use MAVEN's ionosphere observations to advance understanding of the ionosphere spatial structure and its controlling agents. The former will explore the connections between solar energy inputs and atmospheric structure with the ionosphere, while the latter will incorporate MAVEN ionosphere observations into an ongoing international effort to develop an up-to-date empirical Mars ionosphere model—such models for the terrestrial and Venus ionosphere have taken on extremely important roles in theoretical understanding of the two planet's ionosphere processes.

Getting into the core of MAVEN's goals (i.e., the measurement of atmospheric escape rates in the current epoch and determining the solar control of their variations, so that one can extrapolate back with the history of the sun to determine where the atmosphere went) systematical investigations of the escaping particle properties are the objectives of the last studies in Table 1. The Combi effort will use updated theoretical models and MAVEN measurements of the hot escaping coronal atmospheric species to determine the escape rate variations. The Seki tasks will explore the relative importance of all the processes that have been isolated as potential sources of the losses of heavy ions from Mars atmosphere. Ma's modeling efforts will develop and run specific magnetohydrodynamic models of the escaping plasmas for many different states of the Sun's activity. These will be available to the MAVEN team for planning and interpretation of the data. Finally, Crary's investigation will explore the loss of atmosphere through direct measurement of pick-up ionization and the source environs, with a much needed advancement in the theoretical modeling needed to understand the process. Details of each investigation will be singled out subsequently in separate sections.

In addition to extending the scope of MAVEN's originally proposed science investigations, the MAVEN Participating Scientist activities will use, and participate as players in planning of MAVEN's instrument activities. Although each of the instruments is described in great detail in separate papers in the Space Science Review MAVEN Special Issue, since they are cited in the ensuing pages of this paper, they are sketched here for completeness:

1. Imaging Ultraviolet Spectrometer (IUVS). Samples profiles of neutrals and ions through limb emissions and stellar occultations and provides maps of D/H and hot oxygen corona.
2. Langmuir Probe and Waves (LPW). Measures electron density, temperature, spacecraft potential and low frequency waves. A separate sensor monitors solar EUV irradiance.
3. Neutral Gas and Ion Mass Spectrometer (NGIMS). Measures in situ composition (including isotopes) of atmosphere and ionosphere.
4. Suprathermal and Thermal Ion Composition Spectrometer (STATIC). Measures composition, velocity and energy distributions of dominant ion species from thermal to ~20 keV energies.
5. Magnetometer (MAG). Samples vector magnetic field from ~0.1 NT to ~60,000 nT.
6. Solar Wind Electron Analyzer (SWEA). Measures energy distribution, pitch angles of electrons from 5 eV to 5 keV.
7. Solar Wind Ion Analyzer (SWIA). Measures proton and alpha particle velocity distributions from less than 50 to more than 2000 km/s.
8. Solar Energetic Particle (SEP) Analyzer. Samples protons, heavier ions and electrons from ~25 keV to greater than MeV energies.
9. Accelerometer Science (ACC). Spacecraft accelerometer (ACCEL) and orientation data are used to deduce profiles of atmosphere density, temperature and possibly neutral winds.

2 The Proposed Studies

2.1 MAGE: Maven Atmospheric Drag and Gravity Experiment

Team: Rosenblatt, P. and Beuthe, M., Royal Observatory of Belgium; Marty, J.C., Centre National d'Etudes Spatiales, Groupe de Recherche en Géodésie Spatiales; Konopliv, A.S. and Castillo, J.C., Jet Propulsion Laboratory, California Institute of Technology

2.1.1 Overview

The two objectives of the Maven Atmospheric drag and Gravity Experiment (MAGE) are to measure in situ the mass density of the Martian atmosphere during low-altitude pericenter passes and to improve the resolution of Mars' static gravity field. The experiment will perform Precise Orbit Determination (POD) of the spacecraft by using the radio-navigation tracking data.

Mars' upper atmosphere density will be inferred on the basis of the precise reconstruction of the drag acceleration imparted to the spacecraft. This method of measuring the mass density of the upper atmosphere completely differs from what other instruments onboard MAVEN will do (e.g. the ACCEL and the NGIMS instruments) and thus provide an independent determination of that parameter. The MAVEN atmospheric mass densities derived from the orbital drag retrieval will add to the long time series obtained by other spacecraft using the same POD method or other methods, thus providing a monitor of Mars' upper atmosphere densities through almost two solar cycles (i.e. 1997–2016). MAGE will thus help

to contribute to the characterization of the present Mars upper atmosphere and to studies of the influence of the solar activity on the atmospheric escape. The MAGE atmospheric density estimates will also be used to cross-validate the ACCEL density estimates and to support calibration of the NGIMS measurements.

The precise reconstruction of the orbital perturbations of the MAVEN spacecraft will allow us to improve the static gravity field model of Mars particularly due to MAVEN's lower periapse altitude (∼150 km) than for previous spacecraft. The stacking of MAVEN tracking data with data provided by other Martian spacecraft like the Viking orbiters, Mars Global Surveyor (MGS), Mars Odyssey (ODY), Mars Express (MEX), and Mars Reconnaissance Orbiter (MRO), will provide the best global solution of Mars' static gravity ever obtained. This updated gravity field will support studies of the geological history of the Martian surface and of the thermal evolution of its interior.

2.1.2 Precise Orbit Determination (POD) Method

The POD method consists in fitting modeled spacecraft velocities perturbations projected onto the Earth-spacecraft line-of-sight (LOS) direction to LOS velocities measured by the X-band Doppler radio-tracking data. The velocity perturbations are modeled using a numerical integration of the orbital motion, which involves a spacecraft force model. This force model takes into account gravitational forces (gravity field of the planet, gravitational attraction of its moons and of the other planets in the solar system) as well as non-gravitational forces that act on the faces of the spacecraft (bus, solar panels and high gain antenna). These surface forces result from the low-altitude atmospheric drag and from radiation pressure (due to photons emitted by the Sun, to reflected light and to thermal infra-red emission of Mars). The spacecraft attitude is maintained by regularly performing specific maneuvers (Angular Momentum Desaturation or AMD) generating spacecraft accelerations that must also be accounted for. A detailed description of the force model for Martian spacecraft is given in Rosenblatt et al. (2008), Marty et al. (2009) and Konopliv et al. (2011). Nevertheless, a perfect force model cannot be achieved because (1) the gravity field is not perfectly known, (2) the fidelity of AMD acceleration modeling is limited, and (3) the modeling of non-gravitational forces depends on poorly known quantities such as the atmospheric density at low altitude. Hence, the least-squares fit of the modeled LOS velocities to the Doppler tracking data aims at improving the force model in order to reconstruct a precise orbit of the spacecraft. In turn, this approach also leads to a better knowledge of the planet's upper atmosphere (mass density) and gravity field (e.g. Mazarico et al. 2008; Marty et al. 2009; Konopliv et al. 2011; Rosenblatt et al. 2012).

2.1.3 Atmospheric Density from Drag

With the POD method one can measure the drag produced by air friction on the spacecraft at each pericenter pass tracked from the Earth. This method has been successfully used in the past for the study of the Martian upper atmosphere (Mazarico et al. 2008 and references therein) and more recently of the Venusian atmosphere with the Venus Express Atmospheric Drag Experiment (VExADE) (see Rosenblatt et al. 2012). Non-gravitational forces (in particular the atmospheric drag), are modeled with the so-called box-and-wings macro model in which the spacecraft is represented by flat plates (6 for the bus and 2 for each solar panel) with known areas and optical properties. Given the orientation of each plate (provided as telemetered quaternions), the drag acceleration imparted to the spacecraft is computed as

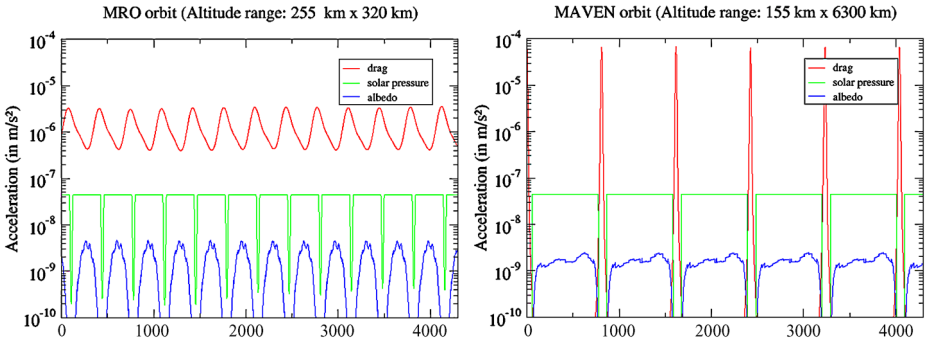

Fig. 2 Predicted non-gravitational acceleration (atmospheric drag, solar pressure and albedo) for a spacecraft with a circular MRO-type orbit (*left panel*), and for an eccentric MAVEN-type orbit (*right panel*). The x-axis is time in seconds and the y-axis is acceleration in m/s^2

the summation of the acceleration $\vec{A}_D$ for each plate exposed to the drag. It is expressed as follows:

$$\vec{A}_D = \frac{1}{2}\rho F_D \sum_{i=1}^{i=N} C_{di} \frac{S_i}{m} (\vec{V}_r \cdot \vec{n}_i) \vec{V}_r \tag{1}$$

where S_i, C_{di} and $\vec{n}_i$ are, respectively, the surface area, the drag coefficient and the normal vector of each plate facing the spacecraft velocity $\vec{V}_r$ relative to the atmosphere, which is assumed to be co-rotating with the planet; m is the mass of the spacecraft, ρ Mars' upper atmosphere density as given by an a priori model (see for example the MARSGRAM model), and F_D is the scale factor of the drag acceleration (or drag scale factor) fitted to the tracking data in the least squares iterative procedure of the POD. The F_D value is then used to scale the atmospheric density value of the a priori model used to compute the orbit ($F_D = 1$ means that the a priori model fits the tracking data). This fitting procedure requires tracking data in the part of the orbit where the drag acceleration can be detected. If the orbit is nearly circular, drag is permanent like for MRO (10^{-6} m/s^2 on average, see Fig. 2—on left), while drag only occurs closely around the pericenter pass for an elliptical orbit like MAVEN (up to 10^{-4} m/s^2 at pericenter, see Fig. 2—on right). The MAVEN tracking coverage is continuous for two successive 4.5 h (orbit period) periods, followed by four without tracking. Thus, it offers the opportunity to provide in situ measurements of atmospheric densities at two successive pericenter passes out of every six, using the POD method.

The precision on the estimated densities depends not only on the precision of the tracking data but also on the quality of the reconstructed orbit and on the error on the computed value of the drag coefficient C_d. The computation of this coefficient is based on several assumptions, corresponding to an overall error of about 25 % (e.g. Rosenblatt et al. 2012 and references therein).

These results obtained with MAGE on MAVEN will be compared to densities derived from tracking data of previous spacecraft, MGS, ODY, MRO, and Mars Express (MEX) in order to provide monitoring of the upper atmosphere densities over almost two solar cycles (although with varying altitude ranges between about 155 km and 400 km as well as varying local time and latitude sampling, see Fig. 3 for the latitudinal and longitudinal repartition of the sampled areas of the upper atmosphere).

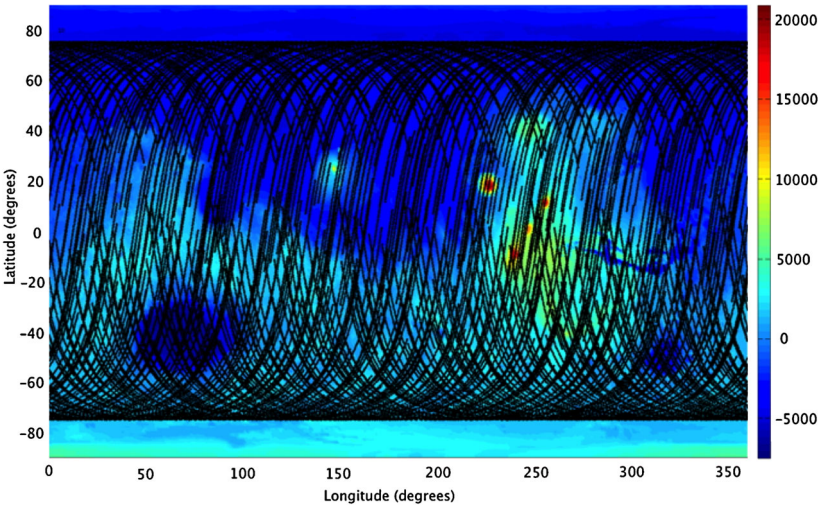

Fig. 3 Projections of MAVEN orbit tracks onto the topographic map of Mars for orbital altitudes lower than 320 km. These tracks correspond to the tracking passes scheduled for the nominal mission (i.e. two successive passes out of every six). It shows the latitudinal and longitudinal sampling of the low-altitude upper atmosphere as well as the areas where the local gravity field will be improved as expected from the MAGE experiment. The *color scale* is for altitudes in meters

2.1.4 Improving Mars' Static Gravity Field

The spacecraft orbit is mainly determined by the gravity of the planet. The gravitational potential U associated with the external planetary gravity field is usually represented as a spherical harmonics series:

$$U = \frac{GM}{r} + \frac{GM}{r}\sum_{l=2}^{l=L}\left(\frac{R}{r}\right)^{l}\sum_{m=0}^{+l}(C_{lm}\cos m\lambda + S_{lm}\sin m\lambda)P_{lm}(\sin\varphi) \qquad (2)$$

where G is the gravitational constant, M is the mass and R the equatorial reference radius of the planet, C_{lm} and S_{lm} are normalized harmonic coefficients of degree l and order m, the P_{lm}'s are the normalized Legendre functions of the first kind (Legendre polynomials when $m = 0$), and r, φ, λ are the spherical coordinates of the point P in a reference system fixed with respect to the planet. The first term in the right-hand side of Eq. (2) represents the central term of the potential and generates the Keplerian motion of the orbiter. The second term represents the potential U_p, which generates perturbations of this Keplerian orbit. The Keplerian orbit and its perturbations are described by the Lagrange planetary equations, which can be solved by perturbative methods, as done by Kaula (1966). This type of solution shows that each gravity field harmonic perturbs the orbital motion with a given dependence on the main characteristics of the orbit, i.e., the semi-major axis, inclination and eccentricity. In particular, some harmonics produce amplified perturbations (or resonances) depending on the spacecraft orbital characteristics. The differences in orbital properties for MAVEN and MRO result in resonances for these orbits at different orders (as for example the orders around 50, 60, 70 and 80).

Study of these resonances will contribute to improving the harmonics of the global solution with respect to the currently existing solution mainly based on MRO, MGS and ODY data. This improvement will be obtained by merging the normal equations inferred from

MAVEN POD with those derived from other spacecraft POD. A significant improvement is expected in particular at short wavelengths since the tracking data of MAVEN offers a good coverage of the planet for low-altitude pericenter passes where the spacecraft is sensitive to short wavelengths gravity perturbations (see Fig. 3).

Two solutions of the gravity field will be computed, one at JPL and one at ROB/CNES, using two different software, the ODP (Orbit Determination Program, Konopliv et al. 2011) and GINS (Géodésie par Intégrations Numériques Simultanées, Marty et al. 2009) respectively. Each solution will be evaluated following established procedures (e.g. spectral analysis, correlation with the topography) and will be compared for cross-validation.

2.1.5 Impact of MAGE

The estimated atmospheric densities will allow us to monitor the variations of mass density in Mars' upper atmosphere with a spatial and temporal sampling determined by the tracking coverage at pericenter and by the drift of the MAVEN orbit. This new series of measurements of the upper atmosphere density will contribute to MAVEN's objective to characterize Mars' upper atmosphere. These results will add to the long time series estimated by the same POD method with other spacecraft over almost two solar cycles, and hence will contribute to the study of the influence of solar activity on the upper atmosphere.

The updated static gravity field of Mars will provide the best solution ever obtained. The ability to well separate the drag signal from the gravity signal with the POD method will be assessed using numerical simulations (as done for the drag signal on the VExADE experiment, Rosenblatt et al. 2012) in order to provide a realistic error on this new gravity field solution. The expected improvement at short wavelengths will help refine geophysical analyses leading to better constraints on the shallow depth interior structure of Mars (crustal densities, lithospheric thicknesses), especially at the volcanic edifices of the Tharsis and Elysium provinces and at the Valles Marineris canyon in order to improve our understanding of the crustal composition and surface thermal flow evolution (e.g. Beuthe et al. 2012), which are essential for the reconstruction of the geological history of the Martian surface.

2.2 Using MAVEN to Characterize Mars Upper Atmosphere Variability and Its Connection to the Lower Atmosphere

Team: England, S., U. California Berkeley; Yiğet, E., George Mason U.

2.2.1 Overview

The dynamics of planetary upper atmospheres are driven by solar radiation, the solar wind and processes occurring at lower levels in those atmospheres. Owing to its important role in mediating atmospheric escape processes, the upper atmosphere of Mars has been the focus of recent research. Mars' upper atmosphere variability is quantified by a variance parameter σ_M (defined here as the sum of periodic variations on temporal scales from minutes to several hours and spatial scales of 100 s of m to 100 s km). This parameter varies dramatically on all measured spatiotemporal scales (e.g. Fritts et al. 2006; Forbes et al. 2002). Results from previous missions have shown that σ_M is strongly correlated with lower atmospheric processes, suggesting that the underlying atmosphere and topography probably influence σ_M (e.g. Forbes et al. 2002). It is known that atmospheric waves transfer a significant amount of energy and momentum from the surface to the upper atmosphere (e.g. Medvedev and Yiğit 2012), however, their role in shaping the variability

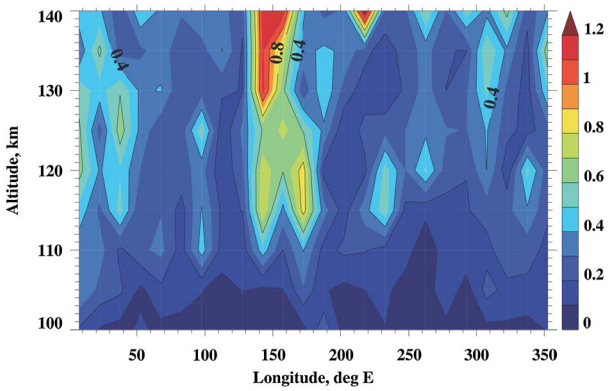

Fig. 4 Lower thermospheric density variances observed by the Mars Odyssey spacecraft, scaled by the mean density in 15° and 5-km bins from orbits 7-134. After Fritts et al. (2006)

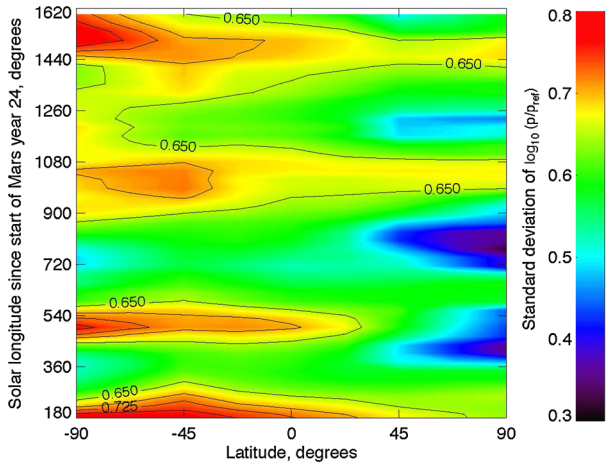

Fig. 5 Mean orbit-to-orbit difference in the observed thermosphere mass densities at 185 km from MGS measurements as a function of solar longitude since the start of Mars year 24 and areographic latitude, shown as the standard deviation of the mass densities relative to a reference density. After England and Lillis (Fig. 10, 2012)

of the Martian upper atmosphere in various scales has yet to be determined. Understanding these waves is an important component of understanding the current state of Mars' upper atmosphere and the processes that control it.

Of all atmospheric waves, it is the small-scale gravity waves (GW) that have the largest momentum flux associated with them. Density perturbations derived from accelerometer data taken by previous missions to Mars has shown that these waves are large in amplitude over certain locations on the planet (see Fig. 4). Assessment of such variability of lower atmospheric origin is necessary to better interpret future observations of the Martian upper atmosphere, such as the ones of MAVEN.

This study is motivated by recent results from England and Lillis (2012), that show that σ_M is consistently higher in Mars' Southern Hemisphere than Northern Hemisphere, regardless of season (see Fig. 5); and that gravity waves generated in the primary wave source region (believed to be close to Mars' surface) can propagate all the way up through all levels of Mars' atmosphere (Medvedev and Yiğit 2012). The significant amplitude of gravity waves at Mars enables them to strongly modulate the dynamics, temperature, and turbulent mixing of Mars' upper atmosphere (Medvedev and Yiğit 2012).

2.2.2 Gravity Wave Importance on Upper Atmosphere

While localized regions of high gravity wave amplitude such as those shown in Fig. 4 are indicative of localized sources at lower altitudes, a simple one-to-one correlation between the topography and σ_M is not seen (Creasey et al. 2006a, 2006b) because filtering by winds affects upward wave propagation, allowing only a certain fraction of the waves generated in the lower atmosphere to reach the thermosphere. To assess the link between σ_M identified in the MAVEN observations and lower atmosphere sources, we will therefore employ a numerical code that tracks atmospheric gravity waves (GWs) from their source to higher altitudes and calculates their dissipation and subsequent influences on the atmosphere. This code takes into account lower atmospheric as well as upper atmospheric physics-based dissipative mechanisms that affect the upward propagation of small-scale GWs and thus forms an unprecedented tool to study GWs in the Martian whole atmosphere system (Medvedev and Yiğit 2012).

The goal of the project described here is to investigate how the lower atmosphere affects the current state of the Martian upper atmosphere and how such vertical coupling can impact the interpretation of MAVEN's measurements.

2.2.3 Science Approach

The study described here will characterize the nature of σ_M and investigate its possible links to wave sources at lower altitudes. This work can only be accomplished with the new observations of atmospheric density and composition from MAVEN. This work must occur during MAVEN's prime mission to both inform the MAVEN team about the variability of the upper atmosphere and to design and execute a short dedicated MAVEN observational campaign to more deeply study σ_M.

The result sought here will have important consequences for MAVEN's quest to understand atmospheric escape variability. The initial observations inferred from Mars Global Surveyor (MGS) electron reflectrometry (shown in Fig. 5) indicated that the short-term atmospheric variability is consistently highest in the Southern Hemisphere, peaking around perihelion, which may have significant implications for studies of atmospheric escape, regardless of the source of that variability. It is possible that the combination of the highest solar irradiance, highest solar wind pressure and Martian Southern Hemisphere summer that all occur simultaneously around perihelion may prove to the perfect storm for atmospheric escape. Thus, while the work described here does not directly address atmospheric escape, characterizing the variability of Mars' upper atmosphere may provide essential insight into MAVEN's core science.

As an integral part of this study, we will work with the NGIMS and IUVS teams to organize an observational campaign to provide the high-resolution NGIMS density measurements required to determine small-scale fluctuations in σ_M. During the campaign, NGIMS will be commanded to perform high-resolution (30 ms) sampling of a single atmospheric species (e.g. CO_2) when MAVEN is below 500 km altitude. This will provide the highest possible resolution density observations. Observations from the stellar occultations with IUVS made on an adjacent orbit will provide insight into the lower levels of the atmosphere (dust opacity, O_3 and CO_2 scale heights) that provide the necessary context for a detailed comparison of the results of this campaign with the modeling work outlined above.

2.2.4 Impact of Study on MAVEN's Science

Determining qualitatively and quantitatively the contribution of lower atmospheric sources to upper atmosphere variability at various temporal and spatial scales is crucial for advancing

the current state of knowledge in planetary atmospheres and for designing better planetary missions in the future. Our research goals target coupling processes in the Martian whole atmosphere and will be achieved in three steps: (1) determine the spatiotemporal scales of upper atmospheric variability observed by MAVEN to better understand the current state of the Martian upper atmosphere, (2) investigate the effects of lower atmospheric small-scale waves on the upper atmosphere, and (3) assess how the lower atmospheric variations influence the upper atmosphere and atmospheric loss. This whole atmosphere approach will have great impact on the understanding of how the upper atmosphere of Mars is influenced from below on various scales.

2.3 The Current State of the Martian Upper Atmosphere: Combining Remote Sensing Observations with in situ Measurements on MAVEN

Team: Stevens, M.H. and Siskind, D.E., Space Science Division, Naval Research Laboratory; Evans, J.S., Computational Physics, Inc., Springfield, VA

2.3.1 Background

The basic state of the Martian atmosphere can vary with latitude, local time, season and solar activity so that its definition implicitly depends on the observation method. The two instruments on MAVEN capable of retrieving the neutral composition are the Imaging Ultraviolet Spectrometer (IUVS) and the Neutral Gas and Ion Mass Spectrometer (NGIMS). Both of these instruments will obtain vertical profiles of major and minor species in the Martian upper atmosphere during each orbit of the planet; however, they will do so in profoundly different ways. IUVS will obtain vertical profiles remotely from the airglow and by stellar occultation, whereas NGIMS will obtain in situ profiles during each elliptical orbit as MAVEN dips down to periapsis.

Although IUVS and NGIMS measure many of the same constituents, operations do not permit them to measure the same air parcels at the same time. Therefore, merging these datasets into a seamless picture of the upper atmosphere can only be done with models that can simulate density variations both spatially and temporally. One resource that can be used for this purpose is a Mars General Circulation Model (e.g. Bougher et al. 2008).

2.3.2 Science Plan

We will analyze mixing ratio profiles of trace species common to the NGIMS and the IUVS airglow datasets including carbon dioxide (CO_2), carbon monoxide (CO), molecular nitrogen (N_2), atomic carbon (C) and atomic oxygen (O) to reconcile any differences. Any persistent difference between the two datasets down to periapsis (120–170 km altitude) will be diagnosed using the Mars General Circulation Model. We will focus on the model's ability to reconcile the IUVS and NGIMS observations through tidally induced variations. The model will be sampled using the projected tangent altitudes of the IUVS limb observations to allow for the most direct comparison possible with both model results and the NGIMS in situ observations. The IUVS limb retrievals are limited to daytime whereas NGIMS can measure at any time of day, so that tidally induced variations from day to night will be an important aspect of the comparisons. To better understand differences between the two instruments we may suggest operations that will benefit the science. For example it might be useful to

point the IUVS to the latitude of closest approach so that the NGIMS measurements could be more directly compared to IUVS retrieval results.

It will also be instructive to direct IUVS observations to areas where there appears to be enhanced wave activity that could lead to the formation of Martian mesospheric clouds. As recently discussed by Spiga et al. (2012), mesospheric ice clouds have now been seen by several recent Mars observational platforms including Mars Express (Montmessin et al. 2006, 2007), Mars Global Surveyor (Clancy et al. 2007), Mars Odyssey (McConnoochie et al. 2010) and Mars Reconnaisance Orbiter (Vincendon et al. 2011). These clouds are the Martian analog to the terrestrial noctilucent cloud (NLC) or Polar Mesospheric Cloud (PMC) phenomena with certain important differences. One important difference is that on Earth, NLCs are high latitude phenomena whereas on Mars they appear concentrated near the tropics where the topography and gravity wave propagation conditions are more favorable (Spiga et al. 2012). We suggest that the enhanced scattering associated with these clouds will be detectable by the IUVS at Mars much as UV instruments at the Earth easily detect NLCs (e.g. Stevens et al. 2010; Bailey et al. 2007).

Clancy and Sandor (1998) made the first suggestion that Martian mesospheric ice clouds are composed of CO_2 although later Clancy et al. (2007) noted that sufficiently cold conditions for CO_2 ice formation were not always apparent. Although often composed of CO_2 ice, some observational evidence also supports a water ice composition for Martian mesospheric clouds (e.g. Määttänen et al. 2013). One interesting implication of mesospheric clouds for MAVEN science is the observation that terrestrial NLCs dehydrate the atmosphere and throttle the flux of atomic hydrogen into the thermosphere. Siskind et al. (2008) reported that the key observational signature was a drop in the atomic hydrogen abundance observed by the SABER instrument on the NASA/TIMED satellite in the summer, which models suggest would not have occurred if clouds were not present. Siskind et al. further note that this could have implications for atmospheric escape since this chemical dehydration could compete with upward transport of hydrogen containing species. In the Martian case, we suggest that it would be interesting to see if the UV limb spectra above these clouds are perturbed, suggesting that mesospheric ice formation can affect the composition at higher altitudes.

Since these mesospheric clouds are attributed to meteorological processes originating in the Martian lower atmosphere, the study will address potentially important variations in the Martian upper atmosphere that are forced from below. Evidence for Martian mesospheric clouds is reported down to about 50 km (Clancy et al. 2007) so that the lowermost tangent altitude for IUVS would need to be modified downward in order to address in a campaign to target this science question if desired.

2.3.3 MAVEN Science Augmentation

Reconciling the NGIMS measurements with the IUVS airglow measurements offers not only an opportunity for cross validation between the instruments but also an opportunity for a better understanding of the present state of the Martian atmosphere. By targeting Martian mesospheric clouds with IUVS we will gain new insight to the coupling of the lower atmosphere to the upper atmosphere. Both of these objectives will add to the MAVEN science, complement the existing team activities and improve the quality of the MAVEN data products.

2.4 Integration of MAVEN Neutral and Plasma Observations

Team: Withers, P., Boston U.; Guzewich, S.D., Goddard Space Flight Center

2.4.1 Overview

Prior to the MAVEN mission, although there is a prolific number of ionospheric electron density measurements from radio occultations from other Mars missions and topside sounding measurements from Mars Express, very little data is available of the fundamental parameters responsible for the relationship of the upper atmosphere and ionosphere. The available data of the most important internal parameters are: just two neutral composition altitude profiles (Nier and McElroy 1977), two ion composition profiles (Hanson et al. 1977), and two ion/electron temperature profiles (Hanson and Mantas 1988) from the entries of the Viking landers; and sparse neutral temperature profiles derived from the neutral scale heights measured on the Viking lander entries, aerobraking orbiters, and UV observations. There are no direct measurements of neutral winds. Our goal is to integrate MAVEN data from multiple instruments to determine how the state of the dayside ionosphere is influenced by the neutral atmosphere, solar flux, and magnetic environment.

2.4.2 Science Approaches

The scientific literature contains many basic theoretical and empirically modeled predictions concerning the ionosphere and neutral upper atmosphere of Mars, particularly as regards coupling between them. Testing these predictions with MAVEN data will lead directly to new understanding about the aeronomy of Mars. A description of the predictions to be studied follows.

First, the topside ionosphere scale height is thought to be related to either the neutral scale height, if vertical plasma transport is suppressed by the magnetic field, or to the plasma temperature if vertical ionospheric plasma transport is not impeded by the remnant or solar wind induced magnetic fields (Schunk and Nagy 2009). Transport controls ionospheric vertical structure above ∼180 km. The topside plasma scale height is a very sensitive indicator of the significance of vertical plasma motion. In the idealized limit that vertical plasma transport is entirely suppressed by horizontal magnetic fields, and the plasma is thus in photochemical equilibrium with the atmosphere, the topside plasma scale height will be twice the neutral scale height. In the idealized limit that plasma transport is unimpeded by magnetic fields, and that vertical diffusive equilibrium is attained the topside plasma scale height will be $\frac{k(T_e+T_i)}{m_i g}$, where k is Boltzmann's constant, T_i and T_e the ion and electron temperatures, m_i the ion mass, and g the acceleration due to gravity. The topside plasma scale height will be on the order of 20 km in the first case (e.g., Fig. 6a) and nearly an order of magnitude larger in the second case (e.g., Fig. 6b).

We shall characterize where and when the topside plasma scale height is controlled by the neutral atmosphere (∼20 km scale height) or the plasma temperature (>100 km scale height). We shall explore how the topside plasma scale height depends on the magnetic field, ion composition, magnetospheric conditions, and other factors, searching for patterns when the structure of the topside ionosphere is "photochemical-like", in diffusive equilibrium, or at different intermediate states. MAVEN data used will be from: NGIMS and LPW (topside plasma scale height); IUVS measurements of CO_2^+ emission (inferred topside plasma scale height); NGIMS and IUVS (neutral scale height); LPW (T_e); STATIC (T_i); and NGIMS and STATIC (ion concentrations).

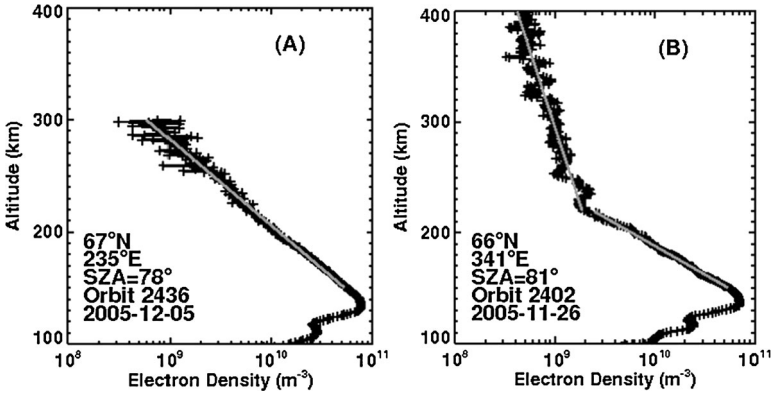

Fig. 6 The lower and upper *gray solid lines* are exponential fits to densities at 150–220 km and 220–400 km, respectively, that have scale heights of 20 km and 120 km. From Fig. 1 of Withers et al. (2012)

Another object of investigation deals with the composition of the topside ionosphere that is thought to be an O^+/O_2^+ mixture, whereas the composition is dominated by O_2^+ at the main peak. Models of the topside composition generally have O^+, O_2^+, and CO_2^+ as the most abundant ions, with the precise mixing ratios varying among models (Najib et al. 2011; Ma et al. 2004; Fox 2004; Shinagawa and Cravens 1992). However, a recent simulation by Matta et al. (2013), that included more comprehensive hydrogen chemistry than in the other models, predicted that HCO^+ may be an abundant ion above 200 km under certain circumstances. The abundances of HCO^+ were greatest when H_2 abundances were high and vertical plasma transport was not suppressed by magnetic fields. Krasnopolsky (2002) also predicted the presence of substantial amounts of HCO^+.

We plan a focused investigation of the HCO^+ abundance because HCO^+ has the potential to play an important role in volatile loss at Mars, by either enhancing or impeding the loss of water. On one hand, if ionized hydrogen exists primarily as heavy HCO^+, rather than lighter OH^+ or H^+, then this will reduce the efficiency with which hydrogen-bearing ions are stripped away from Mars. On the other hand, when HCO^+ is neutralized by dissociative recombination into H and CO, the resultant H atom is suprathermal and highly likely to escape. We shall explore how the HCO^+ abundance depends on neutral composition (especially H_2, O, CO, and CO_2) and the efficiency of vertical transport (inferred from ion velocities, the magnetic field, and the ionospheric vertical structure addressed above. We shall use MAVEN data from NGIMS and IUVS (neutral densities); NGIMS and STATIC (ion densities); STATIC (ion velocities); MAG (field direction and strength); and LPW and NGIMS (ionospheric vertical structure).

Further, studies of the peak electron density have shown that it is a function of solar flux, neutral scale height, and the electron temperature. For idealized conditions, the peak electron density, $N_{\max}$, satisfies Eq. (3) (Withers 2009), where F is the ionizing solar flux, $\alpha = 2.4 \times 10^{-7}$ cm^{-3} s^{-1}, e is 2.718…, H is the neutral scale height, and T_e (degrees K) is the electron temperature and SZA is the solar zenith angle.

$$N_{\max}^2 = \frac{F \cos \mathrm{SZA}}{\alpha e H (300/T_e)^{0.7}} \tag{3}$$

The ion production rate at optical thickness τ equals $\sigma n F e^{-\tau}$ where σ is the absorption cross-section of carbon dioxide and n is the neutral number density, Peak production occurs where $\tau = 1$, or $\sigma n H / \cos(\mathrm{SZA}) = 1$. The ion loss rate equals αN^2 where α, the

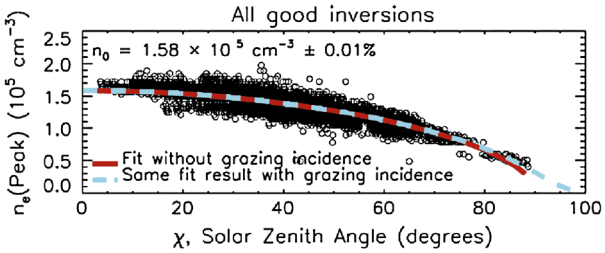

Fig. 7 Peak electron densities observed by the MARSIS instrument are shown as a function of solar zenith angle (from Fig. 4 of Morgan et al. 2008). Only high quality data points ("good inversions") are shown. In the fit to a model that neglects the curvature of Mars ("without grazing incidence"), peak densities are proportional to the square root of the cosine of solar zenith angle and the resultant subsolar peak density, n_0, is 1.58×10^5 cm^{-3}. In the fit to a model that considers the curvature of Mars ("with grazing incidence"), the cosine of solar zenith angle is replaced by a more sophisticated geometrical function that better accounts for the planet's spherical shape

dissociative recombination coefficient for O_2^+, equals $(300/T_e)^{0.7} \times 2.4 \times 10^{-7}$ cm^3 s^{-1}. In photochemical equilibrium, the ion production rate equals the ion loss rate, which leads to Eq. (3).

Prior work (Fig. 7) shows that Eq. (3) is roughly satisfied at Mars (Morgan et al. 2008)—failures indicate areas where understanding is currently weak, needs more study and may yield discoveries. For instance, it will fail in regions where the ionosphere does not have the predominantly O_2^+ composition generally anticipated or in regions where ionization by particle precipitation is an important process. Equation (3) also provides a way to cross-calibrate instruments by testing its accuracy using independent $N_{\max}$ and H data. For instance, if the equation is satisfied using LPW's deduced $N_{\max}$, but not NGIMS's collocated measurements, then the absolute calibration of NGIMS would be suspect. Or, if both $N_{\max}$ measurements agree, and NGIMS, ACC, and IUVS neutral measurements agree, and F is validated against data from Earth during opposition, then Eq. (3) can be used to establish confidence in LPW's measurements of T_e. We shall use MAVEN data from NGIMS, LPW ($N_{\max}$), LPW EUV measurements), ACC, IUVS (Scale height); LPW (T_e). Constraints on $N_{\max}$ are also possible from IUVS measurements of emissions by CO_2^+. Viking composition data indicate that the abundance of this ion is proportional to electron density. If verified by MAVEN, remote CO_2^+ emission data can be converted into electron densities. The ionizing solar flux, F, will be derived from MAVEN's empirical estimate of the solar spectrum constructed by data from the three channels of the LPW EUV sensor.

Finally the last prediction to be tested is that the peak ionosphere altitude is thought to occur at a fixed atmosphere pressure. The main peak is thought to occur at optical depth of unity for ionizing photons, which is equivalent to a pressure level p_m that depends on SZA as $p_m = p_0 \cos(\mathrm{SZA})$, where p_0 is the pressure at the subsolar peak altitude (Chamberlain and Hunten 1987). In the simplest possible representation, p_0 equals mg/σ, where m is the mean molecular mass of CO_2 (44 Daltons), g is the acceleration due to gravity and σ is the absorption cross-section of CO_2, with a suitable characteristic value of $\sim$2–3 $\times 10^{-17}$ cm^2 (Schunk and Nagy 2009). This corresponds to $p_0 = 8$–12×10^{-5} Pa.

However, there are no current simultaneous measurements of pressure and plasma density, so the extent to which the underlying assumptions are satisfied has not been established. Deviations from these expectations indicate areas where understanding is currently weak and discoveries are possible. We shall investigate where and when the pre-

dictions for p_m and p_0 fail (e.g., by variations in observed electron temperature or ion chemistry) by using LPW (ionospheric density near the peak altitude) to estimate the peak altitude and NGIMS (neutral mass densities) profiles to find the corresponding pressure.

2.4.3 Contributions to Mission Planning

This project will contribute to mission planning and mission operations by the cross-calibration of data from several different instruments, which will build confidence in data quality, and will identify of regions and conditions where the ionosphere behaves unusually, which will influence MAVEN's observing strategies.

2.5 Semi-empirical Modeling of the Martian Ionosphere and Its Day-to-Day Variability

Team: Mendillo, M. and Narvaez, C., Center for Space Physics, Boston U.

2.5.1 Introduction

The aeronomy of Mars and atmospheric loss involve a complex blend of neutral and plasma processes driven by internal mechanisms, as well as by important couplings from above and below (see the Aeronomy paper in this special issue). MAVEN offers a comprehensive set of measurements for the entire system: input parameters, intermediate states, and final effects. The most direct manifestation of solar irradiance effects is upon the ionosphere—simply because photo-chemistry is the dominant aeronomical process for Mars' neutral-plasma components. Historical patterns are available for (a) the maximum electron density ($N_{\max}$) of Mars' ionosphere from topside radio soundings and radio occultation profiles; other methods give the integral of the Martian electron density profile, $N_e(h)$, called total electron content (TEC). How can MAVEN-detected ionospheric densities and escape of plasma from the topside ionosphere be assessed without prior knowledge of how the ionosphere plasma is known to vary? The Participating Scientist effort described here offers new ways to assess MAVEN data sets in ways tailored to enhance the science return of the mission. The approach offered is to incorporate MAVEN data in a COSPAR-sponsored Mars International Reference Ionosphere (MIRI).

2.5.2 Organization of MIRI and Its Preliminary Use for Context

Maximum Electron Density The international effort to create MIRI commenced at the COSPAR general assembly meeting in August 2014 in Moscow, Russia. Earlier efforts led by the Boston University MAVEN PS team to achieve a proto-type MIRI resulted in a model for $N_{\max}$ (Mendillo et al. 2013a). The basis of this MIRI-Mark-1 is a set of observations made by the Mars Express radio experiment called MARSIS (Mars Advanced Radar for Subsurface and Ionospheric Sounding). The MARSIS *Active Ionospheric Sounder* (*AIS*) mode (Gurnett et al. 2005) provided ~113,000 determinations of $N_{\max}$ over the years 2005–2012. They were analyzed within the theoretical framework of photo-chemical equilibrium and the resulting semi-empirical model generates $N_{\max}$ for any date back to 1965 for retrospective comparisons with data. Figure 8 shows results from the model in both its retrospective mode (comparison with Viking observations), and its predictive capabilities (for the time of MAVEN's orbital insertion). The MIRI-Mark-1 can be accessed at the Boston University website http://sirius.bu.edu/miri.

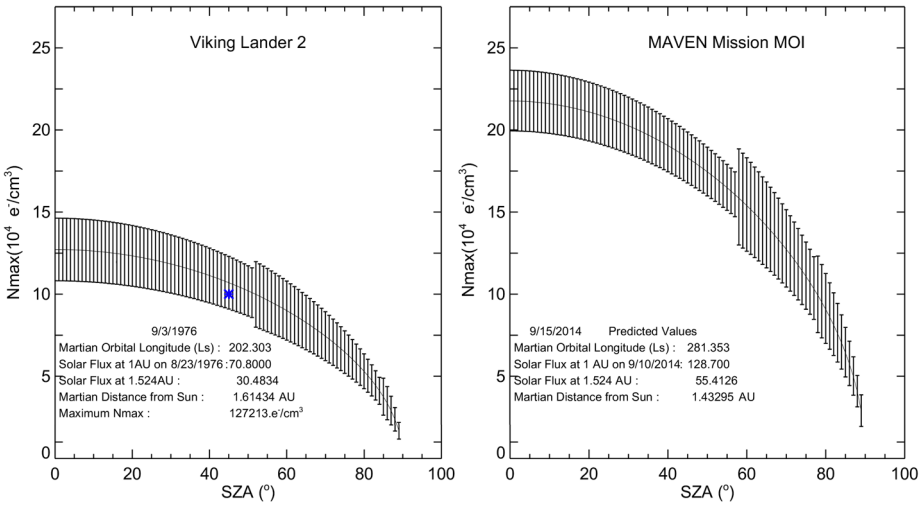

Fig. 8 (*Left panel*) Peak electron density vs. solar zenith angle from MIRI for the day of the Viking-2 landing on Mars (3 Sep. 1976). The $N_{\max}$ measured by the descending lander is shown by the blue asterisk. The solar flux is based on that measured at Earth (23 Aug. 1976) taking into account solar rotation effects between the orbital positions of Earth and Mars. (*Right panel*) MIRI $N_{\max}$ for a predicted date of MAVEN's Mars orbit Insertion. Uncertainty levels in the *left panel* are standard deviations of the input data that created MIRI; the *right panel* also includes prediction uncertainties of solar fluxes. The jump in uncertainty near SZA = 55° reflects an increase in the uncertainty levels of data used to derive the model as SZA increases; for predictions, additional uncertainties arise from predicted solar fluxe (see Mendillo et al. 2013a)

Ionospheric Variability A statistical module within MIRI for the day-to-day changes of the ionosphere at Mars (see review by Withers 2009) has also been started. The initial version used ∼1.2 million TEC values obtained from the MARSIS *sub-surface (SS)* radar (Picardi et al. 2005) spanning the years 2005–2007. Ionospheric variability was characterized by the standard deviations (σ) of mean values of TEC sorted by location on Mars. As described in Mendillo et al. (2013b), there are very significant day-night differences between the variability of the overall plasma content of the Martian ionosphere. This is to be expected because Mars' ionosphere behaves as a terrestrial-type "E-region" (a molecular ion plasma—with very fast recombination chemistry and different day-night ionization sources), and because small changes in low nighttime values yield large variabilities in percent.

The global daytime average variability of the TEC of Mars' ionosphere is ∼20 %, and the nighttime variability is ∼80 %. These represent the first specifications of overall ionospheric variability at Mars using a global database. Given that the TEC is dominated by electron densities at the height of $N_{\max}$ and above, this is a specification that is highly relevant for MAVEN's goal of studying plasma escape from the topside ionosphere.

To quantify the influence of the Martian crustal magnetic fields (**B**) upon ionospheric variability, longitude-latitude regions were selected corresponding to where strong remnant **B**-fields exist versus where low-**B** prevailed. Figure 9 shows the TEC zonally-averaged variabilities in each region. Dramatic differences are found at night—with the high-**B** region variability (>90 %) more than double that in the low-**B** pattern (∼45 %). There is also considerably more structure of σ (TEC, %) versus latitude in the high-**B** sector that correlates with the morphology of the magnetic fields (horizontal vs. vertical).

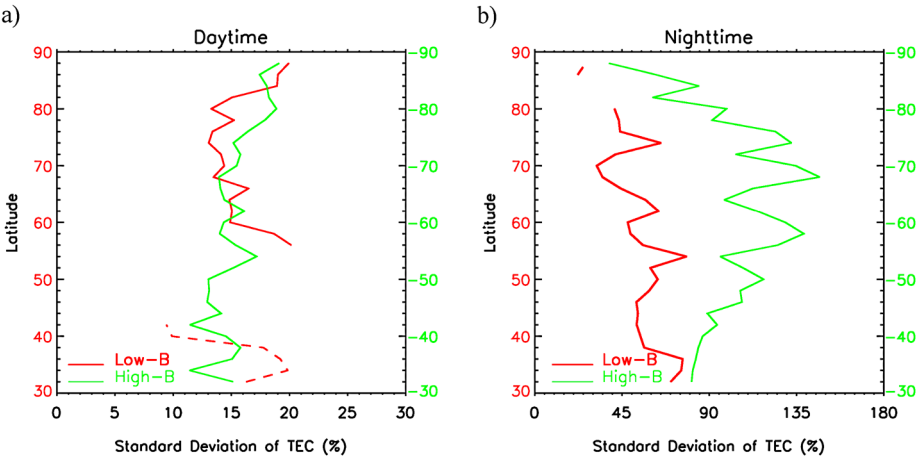

Fig. 9 Latitude profiles of σ (TEC, %) for high-**B** and low-**B** regions. (**a**) Daytime results are given by the *solid green line* (*right axis*) for the high-**B** region and by the *solid red line* (*left axis*) for the low-**B** region. (**b**) Nighttime results using the same format. *Dashed line* segments refer to results where data coverage is sparse. The TEC data come from the Mars Express mission, using the MARSIS radar in sub-surface mode. The regions of interest, containing strong and weak magnetic fields extend from lower mid-latitudes (~30°) to the poles in each hemisphere

2.5.3 Contribution of MAVEN Observations to MIRI

Under the MAVEN PS program, a Mark-2 version of the model will use the photochemistry-plus-plasma-diffusion code described in Mendillo et al. (2011) to produce normalized *shapes* of $N_e(h)$ profiles versus SZAs. When re-calibrated by the MIRI Mark-1 $N_{\max}$ values, estimates of the full electron density profiles will be available. MAVEN observations at various heights will be compared with the climatological MIRI values—the first steps in using in situ and remote sensing data sets for validation. Further validations for MIRI will deal with *episodic conditions*—dust storms, coronal mass ejections, solar flares and active regions, energetic particles, and atmospheric waves and tides. MARSIS TEC data for 2007–2010 will also improve MIRI's statistical module.

The ultimate goal of the MAVEN PS plan described here is to enhance MIRI by incorporating MAVEN's new data sets. In addition to electron densities, plasma temperatures and ion composition are needed. To date this has only been possible for the Earth's ionosphere, and thus MAVEN's contributions will be revolutionary. The Viking descent probes furnished only two altitude profiles of ion composition and ion temperatures (with only a few ion species measured), and only a single profile of electron temperature. All models of the Martian ionosphere rest upon those limited data. MAVEN will provide the first comprehensive set of observations of Mars' plasma properties using modern instrumentation with much higher resolution capabilities.

2.5.4 Summary

The initial phase of the proposed study will be for MIRI to provide context for the evaluation of emerging data sets from the MAVEN instrument. The second phase will use MAVEN data to improve MIRI via validation studies. The final phase will incorporate the full set of

MAVEN observations into an expanded and improved MIRI using capabilities that did not exist prior to the MAVEN mission.

2.6 The Distributions and Escape Rates of Atomic Neutrals from the Upper Atmosphere of Mars

Team: Combi, M.R., Tenishev, V., and Bougher, S., U. Michigan; Schneider, N., U. Colorado, Boulder

2.6.1 Background

The hot atomic coronae in the exosphere of Mars are important for understanding the overall interaction of the solar wind with Mars, the structure of the upper atmosphere, current escape rates from the atmosphere, and their relation to its long-term evolution. Originally the hot coronae of Mars had been modeled using Venus as an analogy. Today the amount of data about Mars' upper atmosphere is still limited; but this will be addressed by a successful MAVEN mission. Gaining a complete understanding of the upper atmosphere of Mars is important and depends on a self-consistent understanding of the generation of the exosphere in the thermosphere and ionosphere, the return flux of the ballistic component of the exosphere back into the thermosphere, the loss from the exosphere, and the interaction of the exosphere and ionosphere with the solar wind. A complete self-consistent modeling capability is necessary to not only investigate the structure and escape rates of the hot atom coronae and their variations in the present epoch over time of year (orbital position) and solar activity, but also to have the capability to extrapolate the escape rates to past epochs to understand the loss of water over several Gyr.

2.6.2 Investigation Plan

To understand the physical and chemical processes important in shaping the tenuous upper atmosphere and exosphere of Mars and the interactions with their particle, field, and radiation environs, it is necessary to employ a physical model that can deal with the rarefied and non-equilibrium, but still collisional, conditions there. With this in mind, the Mars Adaptive Mesh Simulator (Mars-AMPS) 3D gas kinetic model based on the Direct Simulation Monte Carlo (DSMC) methodology (Valeille et al. 2009a, 2009b, 2010a, 2010b) will be applied in combination with the Mars Global Ionosphere Thermosphere Model (M-GITM) (Bougher et al. 2014). The objective is to study the region of the upper thermosphere where the exosphere is generated and to model the entire exosphere and calculate escape rates using use our exosphere Mars-AMPS model in combination with M-GITM, and MAVEN measurements. In particular we will:

1. Interpret MAVEN measurements of the distribution of the hot atomic species throughout Mars' thermosphere and exosphere,
2. Understand their variation during the current epoch with variable conditions, namely solar EUV variations and Mars' orbital position, To calculate the escape rates of hot atoms during the present time,
3. Calculate the structure of the exosphere and the escape rates of atoms during the present time, and
4. Use this knowledge to calculate the changing structure of the exosphere and the escape rates of atoms over geologic time to estimate the water loss from Mars over the history of the solar system.

This investigation builds upon already existing models as part of a multi-faceted approach to achieve a comprehensive understanding of the upper atmosphere, exosphere, ionosphere and interaction of Mars with the solar wind.

This investigation will use a number of standard data products from several MAVEN instruments, namely (1) O, H and C column density distributions by IUVS, (2) altitudinal O, CO, CO_2 and N_2 density distributions with altitude by NGIMS, (3) thermal ion O_2^+ and CO^+ density distributions by NGIMS and STATIC, and (4) thermal electron density and temperature distributions with altitude by LPW. The O, H and C measurements by IUVS and NGIMS will be analyzed directly using our exosphere model. The ion and electron measurements are input quantities for the model, adopted through a self-consistent M-GITM model. The standard data products from IUVS are limb scans of the column abundances of the various species. This investigation also plans to assist in the inversion of IUVS spectra to column abundances that requires a model that accounts for opacity effects (especially important for O at 130.4 nm).

The capabilities of calculating exosphere distributions using various modeling approaches including semi-analytical (Nagy and Cravens 1988; Nagy et al. 2001) and Monte Carlo 1D-spherical models (Fox and Haç 2014) and fully 3D models integrated with 3D thermosphere models (Yagi et al. 2012) were already present on the original MAVEN team. However, since the main mission objectives require a model analysis of the upper atmosphere measurements in order to calculate escape rates, having multiple modeling teams is of the utmost importance to separate the potential effects of model differences caused by model methodology, model assumptions, and input parameters. Furthermore, the members of this investigation team had already been collaborating with MAVEN Co-Investigators on these same problems for a number of years, so all of the modeling tools and interfaces have already been built, tested and applied. The exosphere model already uses both the old and new version of MTGCM and M-GITM (Bougher et al. 2006, 2008, 2009) that are used by the MAVEN mission for investigating the 3D structure of the thermosphere/ionosphere region.

Figure 10 shows the hot oxygen densities derived for six projected MAVEN orbit trajectories for solar minimum equinox (Valeille et al. 2009b). Despite the noise introduced by the Monte Carlo statistics, which will be improved in the future because of a number of improved efficiencies now in the code, one can clearly see the differences in the O density with different orbits at different local mean times that result from a full 3D model.

The calculation uses outputs from the MTGCM, namely, O_2^+ and electron temperature and densities for the hot O source, as well as thermospheric (thermal) O and CO_2 distributions for collisional quenching of the initial hot O distribution to calculate both ballistic and escaping components. This represents a full end-to-end exercising of the same model analysis that will be used as part of this investigation to analyze and interpret MAVEN measurements by IUVS and NGIMS, with the exception that we will be using M-GITM instead of MTGCM and "all" the major neutral species, including CO and N_2, for the collisional background.

A major goal of this investigation is to use the analysis of MAVEN measurements to develop a comprehensive picture of major sources of the upper atmospheric loss processes and their dependence on Mars' orbital position and solar activity. This information will enable projection backward in time to estimate the historical loss of Mars' atmosphere. Figure 11 shows the results from Valeille et al. (2009b) of the hot oxygen density calculations at epoch 1 (the present), epoch 2 (~2.7 Gyr ago) and epoch 3 (~3.6 Gyr) for the loss of hot oxygen from dissociative recombination of O_2^+. Solar conditions were varied in the MTGCM thermosphere/ionosphere model for the 3 different epochs and the 3D exosphere model was run for each of them. The current plan is to expand and improve on these calculations.

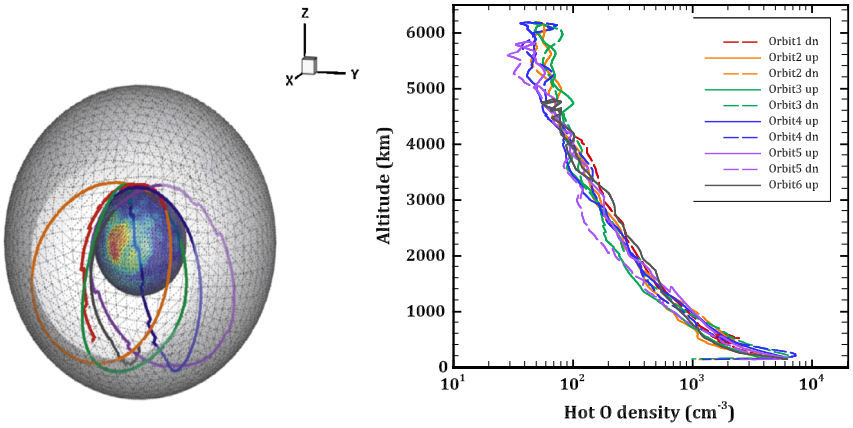

Fig. 10 Modeled hot oxygen density along six MAVEN orbit trajectories. On the left are six orbit trajectories selected for MAVEN science team planning; north is up and $+x$ points to the Sun. On the right are hot oxygen densities calculated with the 3D DSMC model using production and background conditions from the MTGCM. One can see the differences in the O density with different orbits at different local mean times that result from a full 3D model. For example at middle altitudes (∼3000 km), the downward part of orbit 5 (*purple dashed line*) is farther from the subsolar point with an O density a factor of more than two below orbits 1 (*red*) and 2 (*orange*)

Recently, a hot carbon model was incorporated into Mars-AMPS (Lee et al. 2014). This is needed to study the variation of the distribution and escape rate of hot carbon as produced by both dissociative recombination of CO^+ and photodissociation of CO over Mars season and solar minimum and maximum conditions. This will be used to analyze and interpret MAVEN measurements of hot carbon in the thermosphere and exosphere of Mars. Work before the beginning of the MAVEN science mission included the construction of a similar model for the production of both thermal and hot hydrogen as part of the M-GITM thermosphere/ionosphere model and the calculation of the distribution and escape rates of hydrogen using the Mars-AMPS model.

2.6.3 Summary

The investigation will use our 3D exosphere model Mars-AMPS model in combination with the 3D M-GITM thermosphere/ionosphere model to interpret and analyze MAVEN measurements of the principal atomic species, O, C and H in the corona of Mars for the purpose of deriving the escape rates of these species over the range of solar conditions anticipated for the MAVEN mission. It will also include analysis of the sources and escape rates of other escaping species and their resultant escape rates.

2.7 Effects of Regional Couplings on the Ionospheric Flows and the Atmospheric Escape from Mars

Team: Seki, K., Nagoya U.; Nagagawa, H., Terada, N., Tohoku U.; Fujimoto, M., ISAS/JAXA; Medvedev, A., Max Planck Institute; Matsumoto, Y., Chiba U.

2.7.1 Background

The cumulative effect of the atmospheric erosion due to external forcing is regarded as one of the plausible candidates for the drastic climate change from warm and wet to cold and

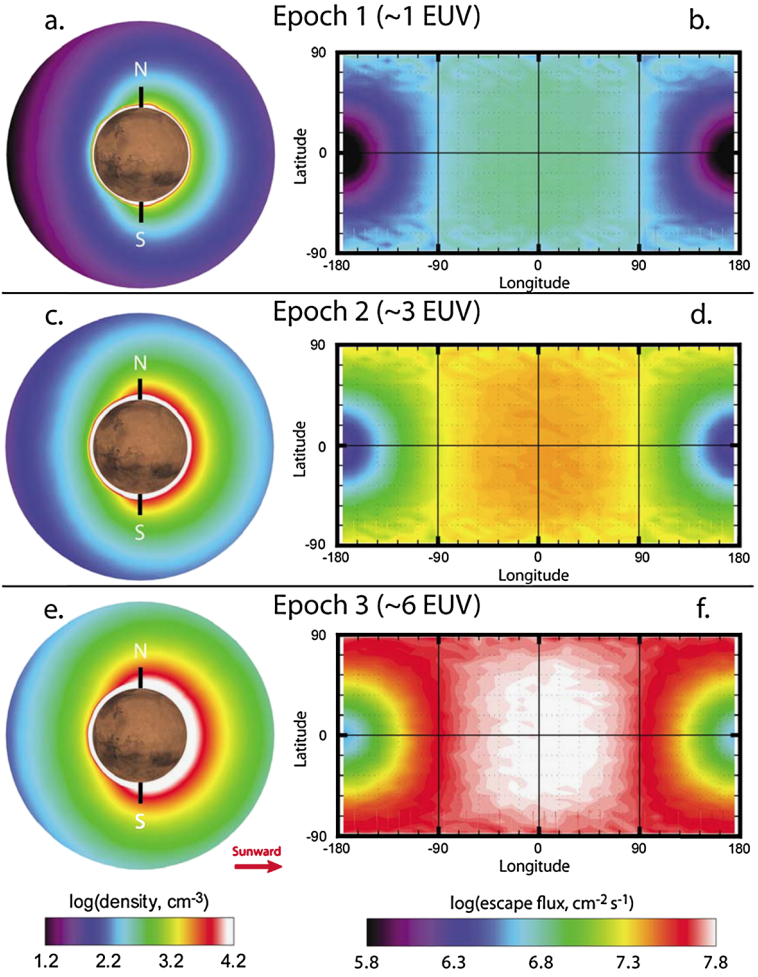

Fig. 11 Hot oxygen density contours (**a**, **c**, and **e**) and hot oxygen escape fluxes (**b**, **d**, and **f**) at 3 Martian radii for epochs 1, 2 and 3, respectively, at Mars equinox and solar minimum conditions (Valeille et al. 2009b). These were calculated with the 3D Mars exosphere model using source and background atmosphere conditions derived from the MTGCM thermosphere/ionosphere model. The *red arrow* indicates the direction to the Sun, and N and S indicate the north and south pole positions of Mars, respectively. The escape rates for the epochs 1, 2 and 3 were 1.9×10^{26} s^{-1}, 2.2×10^{26} s^{-1} and 5.7×10^{26} s^{-1} respectively

dry environment, which Mars is believed to have undergone in the past. There have been proposed a variety of processes of the atmospheric escape from Mars (e.g., Shizgal and Arkos 1996; Chassefiere and Leblanc 2004). Among the candidate escape processes, the solar wind-induced cold ion outflow is pointed out to have a potentially significant contribution to total atmospheric escape from Mars (e.g., Lundin et al. 2009), while it involves substantial uncertainties by previous measurements and theoretical studies (e.g., Dubinin et al. 2011; Lundin 2011; Harnett and Winglee 2006; Ma et al. 2004).

One of the important findings of the Mars Express mission is the significant amount of heavy molecular ion escape from Mars. Carlsson et al. (2006) showed that the escape flux of O_2^+ is comparable to that of O^+, and CO_2^+ flux is about 1/5 of them. It is difficult to pull out

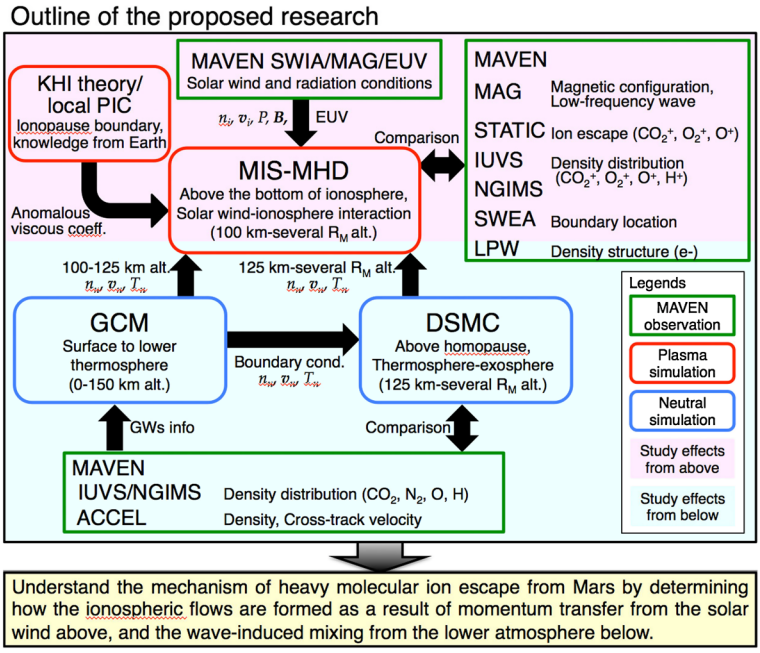

Fig. 12 Outline of the research plan described in Sect. 2.7. Research parts in Sects. 2.7.2 and 2.7.3 correspond to *pink* and *light blue color parts* in the figure, respectively. The relative importance of the two research areas will be compared to achieve the final goal of the research shown at the bottom of the figure

these species from the bottom of the upper atmosphere, unless there is some mechanism to transport CO_2 molecules to high altitudes in the thermosphere to provide a source of CO_2^+ ions. One of the possible scenarios is upward transport of CO_2 due to enhanced diffusion caused by gravity waves (GWs) of lower atmospheric origin.

Once the CO_2 molecules are transported to high altitudes, it will raise the CO_2^+ mixing ratio in the middle ionosphere. Then, ionospheric flows driven by momentum transfer from the solar wind to the ionosphere may eventually pull out the CO_2^+ ions into interplanetary space through cold ion outflows through MHD processes. The outflow rate of CO_2^+ ions thus depends largely on the extent of the solar wind momentum and magnetic field penetration. In order to understand the mechanism that enables the heavy molecular ions to escape from Mars, it is essential to determine how the ionospheric flows are formed as a result of momentum transfer from the solar wind above, and the wave-induced mixing from below.

The MAVEN mission will provide a new set of data to address this question. It observes the neutral source (IUVS/NGIMS/ACCEL), ionosphere (NGIMS/MAG/STATIC/IUVS), solar wind (SWIA/MAG), and escape of the heavy ions together with essential plasma parameters (STATIC/SWEA/MAG/LPW). This PS research contributes to the MAVEN mission by investigating effects of these regional couplings on Martian ionospheric flows and resultant heavy ion escape based on a unique set of the original neutral and plasma simulations (local PIC, MIS-MHD, DSMC, and GCM) and integrated data analysis of the above set of plasma and neutral atmospheric observations by MAVEN. We set three specific targets to achieve the goal. The outline of the research described in this subsection is summarized in Fig. 12.

2.7.2 *Role of KHI and Magnetic Field Penetration in Ionospheric Flows and Atmospheric Escape*

Ionospheric flows driven by momentum transfer from the solar wind to the ionosphere are considered as a driver of cold ion outflows from Mars. To pull out the CO_2^+ ions to interplanetary space, the momentum transfer must reach the lower ionosphere where the CO_2^+ ions are abundant. Limited information provided by the Viking observations indicates that the O^+ and CO_2^+ abundances become comparable at ~210 km altitude (Hanson et al. 1977). On the other hand, the ionopause, the boundary between the draping magnetosheath plasma (induced magnetosphere) and ionosphere, is usually located above 300 km altitude (e.g., Mitchell et al. 2001). The outflow rate of CO_2^+ ions thus depends largely on how deeply into the ionosphere the solar wind momentum and magnetic field penetration can reach.

A viscous type interaction between the shocked solar wind and the ionospheric plasma has been considered as one of plausible candidate mechanisms to cause the penetration (e.g., Terada et al. 2002; Penz et al. 2004; Halekas et al. 2011). Terada et al. (2002) pointed out that the interplanetary magnetic field (IMF) orientation could control the development of the Kelvin-Helmholtz instability (KHI) and cause large undulations of the ionopause. There have been several observations to show the wavy structures of the ionopause (e.g., Halekas et al. 2011). It is also observationally shown that the magnetosheath-like electrons sometimes have access to the 400-km altitude depending on IMF orientation (Brain et al. 2005).

The comprehensive plasma measurements by MAG, STATIC, SWEA, SWIA, and LPW onboard MAVEN will provide the necessary inputs for investigating the mechanism for heavy molecular ions to escape from Mars. The effects of KHI and magnetic field penetration into the ionosphere on the ionospheric outflows will be modeled using our kinetic plasma simulations (local PIC) (e.g., Matsumoto and Seki 2010) and global Multi-Ion-Species MagnetoHydroDynamic simulations (MIS-MHD) (Terada et al. 2009a, 2009b). The modeled results will be compared to the plasma measurements by MAVEN to clarify the efficiency of momentum transfer, its dependence on the solar wind conditions, and its effects on the cold ion outflows from Mars.

2.7.3 *Investigation of the Role of Gravity Waves from the Lower Atmosphere*

In addition to the momentum transfer from the solar wind, an enhanced transport of CO_2 molecules to high altitudes in the Martian thermosphere is required to account for the large amount of CO_2^+ escape observed by Mars Express. Large-scale winds and eddy diffusion are responsible for the main transport effect in the Martian thermosphere. GWs are important in defining large-scale winds and eddy diffusion. Momentum deposited by gravity waves upon their breaking and/or dissipation alters the global meridional circulation, thus affecting mean zonal winds through the Coriolis force and changing mean temperature via the thermal wind relation. Figure 13 is an example of the results of our Martian general circulation model (GCM), illustrating how large-scale winds in the mesosphere and thermosphere are modified by the drag due to GWs propagating from the lower atmosphere. On the other hand, GWs in the Martian thermosphere have been found to be highly variable in space and time (Creasey et al. 2006b; Fritts et al. 2006).

The effects of GWs for the typical conditions of MAVEN observations will be explored by a study of couplings with the upper atmosphere through numerical simulations: (1) Simulation of neutral atmosphere from the planetary surface up to ~150 km altitude with a Martian GCM (Medvedev et al. 2011; Medvedev and Yiğit 2012), (2) kinetic modeling of the

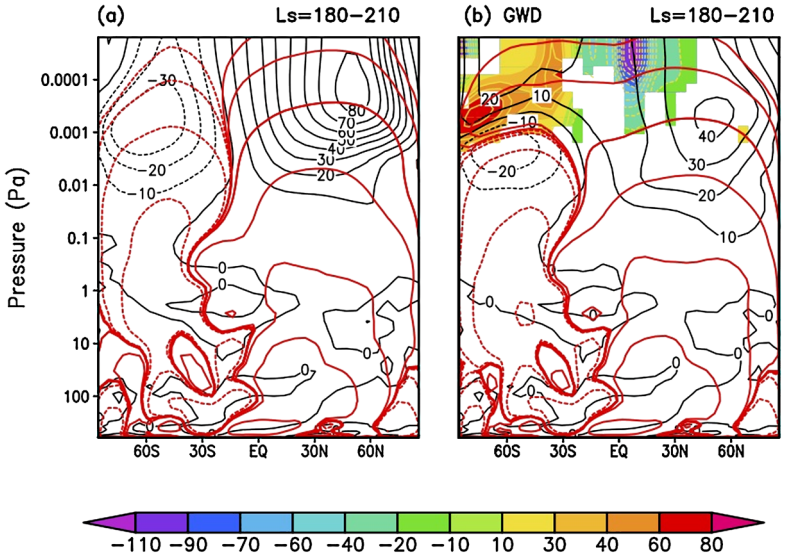

Fig. 13 GCM runs without (*left*) and with (*right*) GWs. *Red curves* are meridional stream functions. *Black contours* denote meridional wind. *Color shade* indicates GW drag. Note that the homopause (∼125 km alt.) is located around ∼0.0001 Pa (Medvedev et al. 2011)

thermosphere and exosphere by Direct Simulation Monte-Carlo (DSMC) simulation (Terada et al. 2014, in preparation), and (3) MIS-MHD simulation of the solar wind-ionosphere interaction (Terada et al. 2009a, 2009b). Simulations with and without GWs will be conducted. Statistical distribution of density variations obtained from the IUVS and NGIMS observations will be used to constrain the GW parameters. The GCM results will be used to determine the lower boundary condition for DSMC, and then the thermospheric and exospheric parameters will be used for the source population of plasma simulated in MIS-MHD. The research described in Sect. 2.2 uses the same gravity wave code. Thus, the inferred wave characteristics can be directly applied to constraining our GCM simulations with the interactively implemented gravity wave parameterization. Further, in our research, we will use this MGCM coupled with the upper atmospheric DSMC and MIS-MHD models to understand the effects of gravity waves in the dynamics of upper atmosphere and ionosphere, where the direct observation data by MAVEN will be available.

The results of the regional coupling simulations will be used to interpret the interpretation of MAVEN remote sensing (IUVS) and in-situ (NGIMS/ACCEL) observations. A combination of our GCM, DSMC, and MIS-MHD simulations will provide quantitative information about the GW-induced density, velocity, and temperature perturbations of CO_2, N_2, O, H, CO_2^+, O_2^+, O^+, and H^+ in the Martian thermosphere, exosphere, and ionosphere, and thus will play a role in the "science closure" of the MAVEN IUVS/NGIMS/ACCEL observations.

2.7.4 Solar Wind and Lower Atmospheric Effects on the Ionospheric Flows and on the Atmospheric Escape

Using the results from the above two investigations as inputs for the global MIS-MHD simulation of solar wind-ionosphere interaction, we will quantify what parameters are

important in defining the ionospheric flows and the escape of ionospheric heavy ions. The results will be compared with magnetic field (MAG), electron density (LPW), and ion (STATIC/NGIMS/IUVS) observations by MAVEN. The escape rates of ionospheric ions (CO_2^+, O_2^+, O^+, and H^+) will be compared with those of neutrals (CO_2, O, and H) inferred from the proposed research in the previous subsection. Through the interdisciplinary coordinated study, we aim to understand the mechanism that enables the heavy molecular ions to escape from Mars by determining how the ionospheric flows are formed as a result of momentum transfer from the solar wind above, and the wave-induced mixing from below.

2.7.5 Summary

Understanding the fate of CO_2 (greenhouse gas) is one of the important questions of the MAVEN mission, which is crucial to unveil the evolution of the Martian surface environment. Our proposed research will quantify what parameters control the ionospheric flows and the escape of the atmosphere, especially CO_2, from present-day Mars. Some of our models (e.g., DSMC and MIS-MHD models) are robust enough to be applicable to the extrapolation backwards in the Sun's history. Therefore, our proposed research will contribute directly to the first and second MAVEN science questions (1) "what is the current state of the upper atmosphere and what processes control it?" and (2) "what is the escape rate at the present epoch and how does it relate to the controlling processes", and also partly to the third question (3) "what has the total loss to space been through time?". The research plan aims at understanding the mechanism of heavy molecular ion escape from Mars by determining how the ionospheric flows are formed as a result of interactions between the solar wind, ionosphere, exosphere, thermosphere, and lower atmosphere based on four sets of simulation models and MAVEN observations (Fig. 12).

2.8 Multifluid MHD Study of the Solar Wind Induced Plasma Escape from the Martian Atmosphere

Team: Ma, Y., UCLA; Nagy, A. and Gabor, T., U. Michigan; Russell, U., California Los Angeles

2.8.1 Background

Even though the nature of the solar wind-interaction with Mars is expected to be similar to that of Venus; the interaction process is more complicated due to its remnant crustal magnetic field (Acuna et al. 1998). The upcoming MAVEN mission will provide an excellent opportunity to further understand this complicated interaction process. However, the spacecraft can only provide measurement along its trajectory, a global model that could self-consistently take into account the effects of the ionosphere, various kinds of collisions and the crustal magnetic field is also needed to provide a global view of the interaction.

The global MHD model for Mars to be used in the study is part of the BATS-R-US (Block Adaptive-Tree Solar-wind Roe-type Upwind Scheme) code (Powell et al. 1999; Toth et al. 2005, 2012), which has been under development at the University of Michigan for more than 20 years. The Mars MHD model (Ma et al. 2002, 2004; Ma and Nagy 2007) has been widely used by the Mars science community (Liemohn et al. 2006, 2007; Li and Zhang 2009; Manning et al. 2011; Li et al. 2011; Curry et al. 2012; Fang et al. 2010; Brain et al. 2010). The recent version of the Mars model (Ma et al. 2004; Ma and Nagy 2007) has very high radial resolution (~10 km) in the ionosphere, which enables the model to reproduce

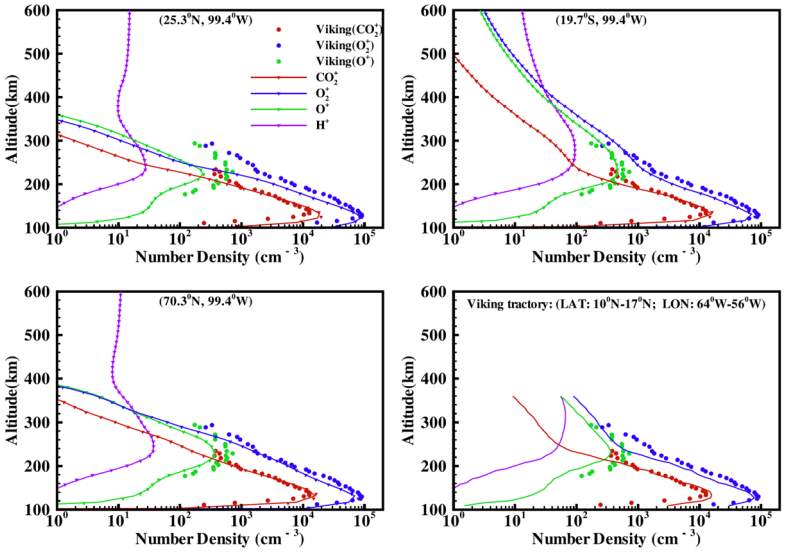

Fig. 14 The calculated solar cycle minimum density profiles for the Viking case along radial lines for different latitudes in the x–z plane. The Viking observations are indicated by the symbols, while the MHD model results are shown by *solid lines*. *Different colors* represent different species (from Ma et al. 2004, Fig. 8)

accurately the locations of various plasma boundaries around Mars, such as the bow shock and the magnetic pile-up boundary (MPB). This fine radial resolution also allows the model to capture the changes of the ionospheric structure due to solar wind interaction. As plotted in Fig. 14, the density profiles vary significantly with location, indicating that the solar wind and crustal field source all have strong influence on the ionospheric structure.

The model has been recently updated to a multi-fluid MHD model (Najib et al. 2011). This new version of the model solves the density, velocity and pressure of proton and three heavy planetary ions (O^+, O_2^+, CO_2^+). The Martian ionosphere is calculated self-consistently based on transport effects induced by solar wind interaction as well as the source and loss terms determined by chemical reaction rates and the preset neutral profiles. The multi-fluid model allows different ion fluids to move at their own velocities and have different temperatures. It is able to reproduce the additional asymmetry along the convection electric field direction, as shown in Fig. 15. The asymmetry in the single fluid model is mainly caused by the crustal magnetic field. The multi-fluid MHD model results show that the velocity patterns are different for different mass ion fluids. The heavier the ion mass per particle, the more significant the flow becomes along the convection electric field direction.

2.8.2 *Investigation*

In this study, we will further improve the current multi-fluid MHD model to include an electron pressure equation to self-consistently calculate the electron temperature. The electron pressure equation included in the improved model can accurately calculate the electron temperature and the electron pressure force. The electron temperature is also needed to calculate rates of some chemical reactions such as dissociative recombination (e.g. $O_2^+ + e \rightarrow O + O$ and $CO_2^+ + e \rightarrow CO + O$) and electron impact ionization that are all depending on the electron temperature. So the improvement of the model is expected to lead to more accurate

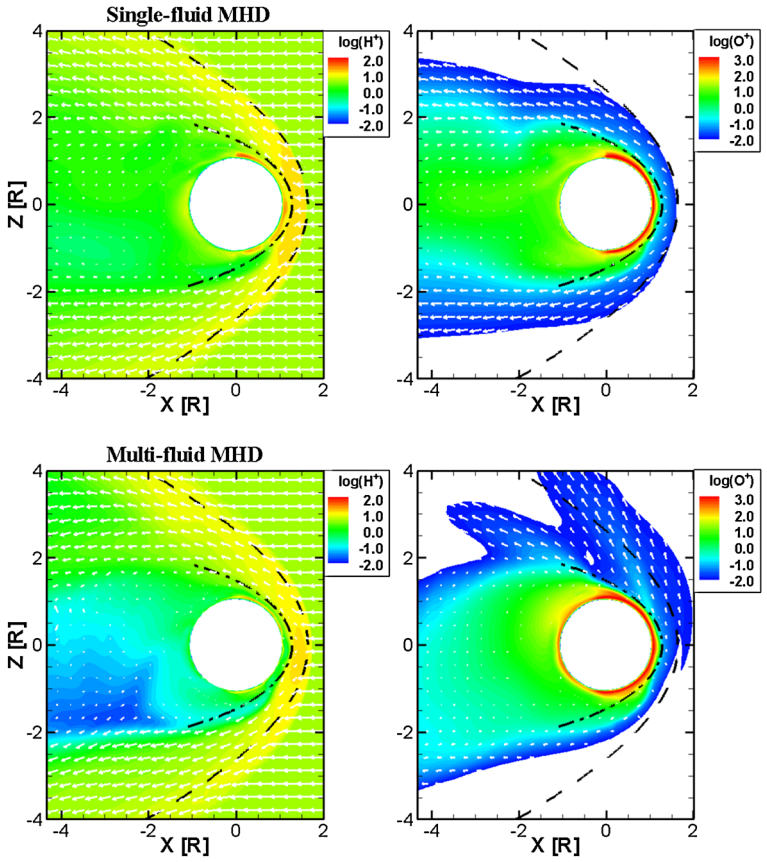

Fig. 15 Density contours of proton and oxygen ion from single-fluid model (*upper two panels*) and multi--fluid model (*lower two panels*). The flow patterns of H^+ and O^+ are the same for the single fluid model, but are significantly different from each other for the multi-fluid model as indicated by the *white arrows*. The *black dashed line* represents the observed mean bow shock and the *dash-dot line* shows the mean MPB location. (Adapted from results of Ma et al. 2004 and Najib et al. 2011.)

evaluation of the ion density in the ionosphere. Similar work has been done for the Titan MHD model (Ma et al. 2011) and it showed that the inclusion of electron pressure equation in the model leads to a significantly improved agreement between the model field and Cassini magnetometer data below the ionopause.

The improved multi-fluid MHD model will be used to locate the most intense region for plasma bulk escape to provide guidance for the operation and data collection of the MAVEN mission. The improved model is also to be used for detailed model-data comparison for a few selected typical orbits of MAVEN (including a few from deep-dip campaigns). We expect that the comparison can provide valuable constraints for the model and lead to a better understanding of the dominant physical processes that are controlling the state of the Martian ionosphere; it can also help to interpret MAVEN plasma data and provide global context for the observations.

The model will also be used to estimate the escape rates of major planetary ions at different stages over Martian history using appropriate solar wind conditions and neutral atmospheric profiles. We plan to simulate each of the 6 solar EUV conditions (ranging from 1

to 100 times the current radiation level) as listed in Table 1 of Boesswetter et al. (2010) using the improved multi-fluid MHD model. The neutral atmosphere profiles for early Mars is from Lammer et al. (2006) for corresponding EUV fluxes. Boesswetter et al. (2010) simulated those cases using a hybrid model but without crustal magnetic field. As we learned from previous studies, the escape fluxes depend on the orientation of the crustal field, so we will run two cases for each condition, assuming that the strong crustal field region is either facing toward the sun or 180 degrees away. The escape fluxes for each of the two cases will be calculated and then averaged to estimate the plasma escape fluxes at different stages of Martian history. The total escape fluxes will also be integrated based on the escape fluxes of the 6 different EUV conditions.

2.8.3 Summary

The object of the study is to use a global multi-fluid MHD model that will be constrained by MAVEN observations to enhance our understanding of the magneto-plasma environment around Mars and to quantify the solar wind induced plasma escape from the Martian atmosphere/ionosphere. Results from the global multi-fluid MHD model for specific MAVEN events will be used to interpret MAVEN plasma data and provide global context for the observations. The improved model will also be used to estimate the escape rates of major planetary ions at different stages over Martian history with appropriate solar wind conditions and neutral atmospheric profiles. MHD model results from different runs will be made available to all MAVEN team members.

2.9 Ion Cyclotron Waves and Pickup Ions as a Measure of Atmospheric Loss

Team: Crary, F., Dols, V., U. Colorado Boulder; Delamere, P., U. Alaska

2.9.1 Background Science

Observations by the Mars Global Surveyor, Mars Express and Phobos 2 spacecraft (Brain et al. 2002; Delva et al. 2011 and references therein) have shown that Mars has a hydrogen exosphere which extends as much as ten Martian radii from the planet. These hydrogen atoms ionize and are "picked up" in the solar wind flow. Neither the associated hydrogen loss rate nor the structure of this extended exosphere, have been well determined.

The resulting pickup protons have a distinctive "ring-beam" velocity distribution and generate low frequency electromagnetic waves near the ion cyclotron frequency. This process has been observed in almost every environment where neutrals are ionized in a flowing plasma. Direct measurements of pickup ions have been made at Mars (Yamauchi et al. 2006), comets (Coates 2004 and references therein), and Saturn (Tokar et al. 2008). Figure 16 shows measurements of pickup ions from the Mars Express ASPERA-3 instrument.

A ring-beam distribution is highly unstable unless damped by a background population of thermal ions, and spontaneously generates electromagnetic waves near the ion cyclotron frequency, $\Omega_i = q_i B/m_i$, where q_i and m_i are the ion's charge and mass and B is the magnetic field strength. These ion cyclotron waves are left-circularly polarized and propagate along the magnetic field. Ion cyclotron waves have been even more widely observed, at Venus (Delva et al. 2011, and references therein), Mars (Brain et al. 2002; Bertucci et al. 2005), comets (Huddleston and Johnstone 1992), Jupiter (Huddleston et al. 2000) and Saturn (Leisner et al. 2006).

These and other, related works show the value of ion cyclotron waves and pickup ion observations: They are a clear indicator of neutral gas being ionized. The wave frequency gives

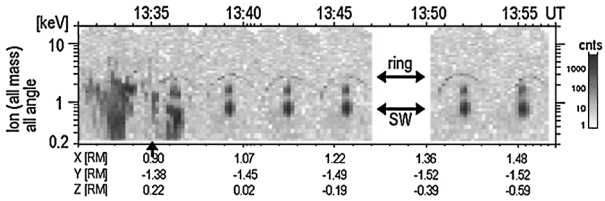

Fig. 16 Mars Express measurements of a ring distribution outside the Martian bow shock. The background solar wind ions are marked "*SW*" and solar wind alpha particles can be seen at twice the energy of the background protons. The ring distribution peaks at four times that of the solar wind protons, which is characteristic of pickup protons (Yamauchi et al. 2006)

the approximate mass of the recently ionized particles. The distribution and intensity of the waves can be used to estimate the distribution of the neutral gas. But making a quantitative link between the observations and the ionization rate or neutral gas density has remained elusive.

2.9.2 Measurements Employed

Observations of the pickup ions themselves are the most direct measure of ion production. Unfortunately, these measurements are difficult and relatively rare. The distinctive pickup ion distribution is superimposed on that of the background plasma. The density of the recently ionized particles is typically much lower than the background density. Since the pickup ions are often the same species as the background ions, even mass-resolving plasma instruments such as MAVEN/STATIC have difficulty separating the pickup from the background. Overall, this makes the direct measurement of pickup ions challenging.

In contrast, ion cyclotron waves are more easily detected. The waves have a narrow frequency peak, occur close to a known frequency and have a specific polarization. Even low amplitudes of under 0.1 nT (3 % of the solar wind field at Mars) are within the sensitivity of magnetometers. This makes high-signal to noise observations of ion cyclotron waves relatively common. In some places outside the Martian bow shock, Brain et al. (2002) reported detections of ion cyclotron waves 50 % of the time Mars Global Surveyor was in that region. This sort of continuous data sets allow studies of the spatial distribution and variability of the parent neutral gas. The primary limitation of studying ion cyclotron waves, and of quantifying the ion production rate, is the wave generation process itself. It is unclear what fraction of the ions' kinetic energy is converted to wave energy, and therefore how to convert an observed wave amplitude to a local ionization rate.

Initial studies of pickup ions and ion cyclotron waves, such as Huddleston and Johnstone (1992), found an approximate analytic form for the scattering of particles by the waves. This allowed them to estimate what fraction of an ion's initial, kinetic energy could be converted to wave energy. Recent numerical simulations (Cowee et al. 2007) have shown that this conversion efficiency may be off by as much as a factor of four. In another context, Saturn's magnetosphere, Leisner et al. (2006), calculated the Poynting flux of the observed waves. They then equated the wave energy propagating away from the source region with the kinetic energy of the freshly produced pickup ions and calculated an ion production rate. It is not clear how accurate this approach is, but it does assume that the observations are made outside the source region and that the direction of wave propagation is known.

In the case of Mars, the problem is more difficult. The growth rate of the waves is typically a small fraction of the wave frequency (e.g. a few percent). Cowee and Gary (2012)

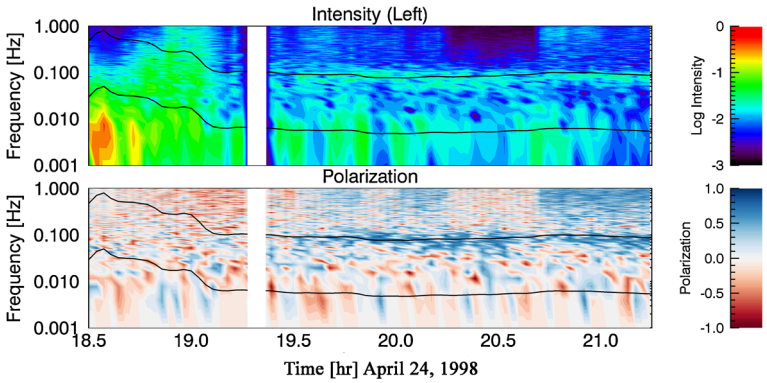

Fig. 17 Examples of ion cyclotron waves observed by Mars Global Surveyor on April 24, 1998. The *top panel* shows the spectrogram computed from the Fourier transform of $B_x - iB_y$ to give the intensity of the left circularly polarized waves. The *bottom panel* shows the polarization, $(I_{\text{left}} - I_{\text{right}})/(I_{\text{left}} + I_{\text{right}})$. *Black lines* indicate the proton and oxygen cyclotron frequencies

using one dimensional hybrid simulations, noted that the pickup ions and the waves they produce will advect far downstream of Mars before the growth process saturates or reaches any equilibrium. As a result, understanding the relation between the waves and the pickup ions is a dynamic process where the evolution of the wave spectrum and the ion distribution must be considered, rather than their initial or final state.

The planned MAVEN analysis of pickup ions and ion cyclotron waves is a three-step process. First, the MAG data will be processed into dynamic spectra. Ion cyclotron waves will be identified (as well as other ultra-low frequency plasma waves). Figure 17 shows an example of this using MGS data and a time interval studied by Brain et al. (2002). From these spectra, the waves' amplitude, peak frequency and other properties are determined. Second, the STATIC data will be examined to identify times when high-quality ion and wave data are both available. Using these intervals as case studies, a combination of theoretical analysis and hybrid simulations will allow us to relate the wave properties to the ion production rate. From this, the exospheric ionization rates can be calculated for all times when ion cyclotron waves are observed.

Based on Mars Global Surveyor observations, we anticipate high-quality data primarily from pickup protons outside the Martian bow shock. This represents 20–40 % of the time when MAVEN's apoapsis is on the dayside of Mars. Inside the bow shock, the plasma environment is highly variable and pickup ions advect through a very heterogeneous environment as they generate ion cyclotron waves. For observations inside the bow shock, we will make empirical comparisons between the wave properties and the pickup ion distributions.

Identification of oxygen cyclotron waves would be of great interest. But it is as technically difficult as it is interesting. The oxygen cyclotron period (∼350 s) in a typical solar wind magnetic field. This makes it unlikely the spacecraft will remain in a more-or-less uniform environment for the tens of periods needed for a clear identification. Closer to Mars, especially over the crustal magnetic anomalies, the cyclotron period will be much smaller. But the environment will also be much more variable and the spacecraft will be moving through it more rapidly. To date, here has only been one, tentative identification of waves at the oxygen cyclotron frequency (Espley et al. 2005). A systematic search for oxygen cyclotron waves will be conducted, but there is no assurance of definitive results.

The instruments on MAVEN will provide the first simultaneous measurements of ion cyclotron waves near Mars and the pickup ions that generate them. Past missions have mea-

sured the waves. Others have measured the pickup ions. But, with the exception of Phobos 2, MAVEN will be the first Mars mission with both a magnetometer and a plasma analyzer. Phobos 2 did not make any simultaneous detections of ion cyclotron waves and pickup ions. Simultaneous measurements are the key to relating wave properties to ionization rates. MAVEN's STATIC instrument will provide compositionally-resolved measurements of the ion velocity distribution with integrated times of 256 seconds or less.

2.9.3 Analysis of Measurements

When pickup ions are identified, we will compare their velocity distribution to that predicted by hybrid modeling. These comparisons will be used to correct and improve the model and its assumptions about pickup production rates and the ionization of the neutral exosphere. This will allow us to accurately estimate ionization rates from ion cyclotron wave data, even at times when direct particle measurements of the pickup ions are not available.

Modeling the generation of ion cyclotron waves by pickup ions requires a complete description of the non-Maxwellian particle distributions of the ion. Hybrid simulations accomplish this by treating ions as discrete particles while modeling electrons as a fluid. The hybrid technique was first proposed by Harned (1982), and the particular algorithms for our code were developed by Swift (1995), and Delamere (2009). In the past, it has been applied to diverse problems including the generation of ion cyclotron waves by pickup in the vicinity of Jupiter's moon, Io.

2.9.4 Summary

The MAVEN data set, combining both magnetic field and ion measurements, provides an excellent opportunity to learn about the structure and loss of the Martian exosphere. The ionization of the neutral exosphere produces pickup ions in a ring-beam distribution. The STATIC instrument will directly measure these distributions, but probably not at all times due to the low flux of these ions. The MAG instrument will measure ion cyclotron waves generated by pickup ions, and will probably do so with a high signal-to-noise and for a large fraction of the time. Combining simultaneous MAG and STATIC measurements with numerical, hybrid simulations will provide the link between the wave measurements and the ionization rate. Such measurements constrain models of the Martian exosphere and its loss to space.

3 Conclusion of Paper

The goal of the MAVEN mission is to assess the physical and chemical processes that govern Mars' current atmosphere in order to guide meaningful extrapolations into its past. That agenda is, arguably, the most ambitious topic ever addressed in the field of *planetary atmospheres*. The ultimate prize—how the gaseous envelope of Mars escapes (currently and in the distant past)—is linked to the fundamental search for the origins and maintenance of life in the Solar System (and beyond). To address such lofty goals, the MAVEN mission is not composed of astro-biology instrumentation designed to detect markers of life nor are its sensors chosen for stand-alone studies. The measurements were chosen to provide an integrated systems approach to investigate the innate coupling processes between solar induced plasma inputs and the atmosphere. The upper atmosphere of Mars is a complex blend of neutral and plasma processes driven by mechanism that are internal to it, as well as by important

couplings from above and below. The *Systems Approach* requires—and MAVEN offers—a comprehensive set of measurements and a science team knowledgeable about the entire system. The addition of the Participating Scientists to the MAVEN team has added further valuable expertise to the MAVEN mission and will facilitate the attainment of MAVEN's ambitious system focused goals.

Acknowledgement Support from NASA's MAVEN Participating Scientist Program is acknowledged for all the studies.

References

M.H. Acuna, J.E.P. Connerney, P. Wasilewski et al., Magnetic field and plasma observations at Mars: initial results of the Mars Global Surveyor Mission. Science **279**, 1676 (1998)

S.M. Bailey, A.M. Merkel, G.E. Thomas, D.W. Rusch, Hemispheric differences in Polar Mesospheric Cloud morphology observed by the Student Nitric Oxide Explorer. J. Atmos. Sol.-Terr. Phys. **69**, 1407–1418 (2007)

C. Bertucci, C. Mazelle, M. Acuna, Interaction of the solar wind with Mars from Mars Global Surveyor MAG/ER observations. J. Atmos. Sol.-Terr. Phys. **67**, 1797 (2005)

M. Beuthe, S. Le Maistre, P. Rosenblatt et al., Density and lithospheric thickness of the Tharsis province from MEX MaRS and MRO gravity data. J. Geophys. Res. **117**, E04002 (2012). doi:10.1029/2011JE00397

A. Boesswetter, Y. Lammer, U. Kulikov et al., Non-thermal water loss of the early Mars: 3D multi-ion hybrid simulations. Planet. Space Sci. **58**(14–15), 2031 (2010)

S.W. Bougher, J.M. Bell, J.R. Murphy et al., Polar warming in the Mars thermosphere: seasonal variations owing to changing insolation and dust distributions. Geophys. Res. Lett. **33**, L02203 (2006). doi:10.1029/2005GL024059

S.W. Bougher, P.-L. Blelly, M. Combi et al., Neutral upper atmosphere and ionosphere modeling. Space Sci. Rev. **139**, 107 (2008)

S.W. Bougher, T.M. McDunn, K.A. Zoldak et al., Solar cycle variability of Mars dayside exospheric temperatures: model evaluation of underlying thermal balances. Geophys. Res. Lett. **37**, L05201 (2009)

S.W. Bougher, D. Pawlowski, J.M. Bell et al., Solar cycle variability of Mars dayside exospheric temperatures: model evaluation of underlying thermal balances. J. Geophys. Res. Planets (2014, in preparation)

D.A. Brain, F. Bagenal, M.H. Acuna et al., Observations of low-frequency electromagnetic waves upstream from the martian shock. J. Geophys. Res. **107**, 1076 (2002)

D.A. Brain, J.S. Halekas et al., Variability of the altitude of the martian sheath. Geophys. Res. Lett. **32**, L18203 (2005). doi:10.1029/2005GL023126

D.A. Brain, J.S. Halekas, R. Lillis et al., A comparison of global models for the solar wind interaction with Mars. Icarus **206**(1), 139 (2010)

E. Carlsson, A. Fedorov, S. Barabash et al., Mass composition of the escaping plasma at Mars. Icarus **182**, 320–328 (2006). doi:10.1016/j.icarus.2005.09.020

J.W. Chamberlain, D.M. Hunten, *Theory of Planetary Atmospheres* (Academic Press, San Diego, 1987)

E. Chassefiere, F. Leblanc, Mars atmospheric escape and evolution; interaction with the solar wind. Planet. Space Sci. **52**, 1039–1058 (2004)

R.T. Clancy, B.J. Sandor, CO_2 ice clouds in the upper atmosphere of Mars. Geophys. Res. Lett. **25**(4), 489–492 (1998)

R.T. Clancy, M.J. Wolff, B.A. Whitney, Mars equatorial mesospheric clouds: global occurrence and physical properties from Mars Global Surveyor Thermal Emission Spectrometer and Mars Orbiter Camera limb observations. J. Geophys. Res. **112**, E04004 (2007). doi:10.1029/2006JE002850

A.J. Coates, Pickup ions at comets. Adv. Space Res. **33**, 1977 (2004)

M. Cowee, S.P. Gary, Electromagnetic ion cyclotron wave generation by planetary pickup ions: one dimensional hybrid simulations at sub-Alfvenic pickup velocities. J. Geophys. Res. **117**, A017568 (2012)

M. Cowee, C.T. Russell, R.J. Strangeway, X. Blanco-Cabo, One-dimensional hybrid simulations of obliquely propagating ion cyclotron waves: application to ion pickup at Io, Io's plasma environment during the Galileo flyby: global three-dimensional. J. Geophys. Res. **112**, 6230 (2007)

J.E. Creasey, J.M. Forbes, D.P. Hinson, Global and seasonal distribution of gravity wave activity in Mars' lower atmosphere derived from MGS radio occultation data. Geophys. Res. Lett. **33**, L01803 (2006a). doi:10.1029/2005GL024037

J.E. Creasey, J.M. Forbes, G.M. Keating, Density variability at scales typical of gravity waves observed in Mars' thermosphere by the MGS accelerometer. Geophys. Res. Lett. **33**, L22814 (2006b). doi:10.1029/2006GL027583

S.M. Curry, M. Liehmohn, X. Fang et al., The influence of production mechanisms on pick-up ion loss at Mars. J. Geophys. Res. (2012). doi:10.1029/2012JA017665
P.A. Delamere, Hybrid code simulations of the solar wind interaction with Pluto. J. Geophys. Res. **114**, 3220 (2009)
M. Delva, C. Mazelle, C. Bertucci, Upstream ion cyclotron waves at Venus and Mars. Space Sci. Rev. **162**, 5 (2011)
E. Dubinin, M. Franz, M. Federov et al., Ion energization and escape on Mars and Venus. Space Sci. Rev. **162**, 173–211 (2011). doi:10.1007/s11214-011-9831-7
S. England, R.J. Lillis, On the nature of the variability of the martian thermospheric mass density: results from electron reflectrometry with Mars Global Surveyor. J. Geophys. Res. **117**, E02008 (2012). doi:10.1029/2011JE003998
J.R. Espley, P. Cloutier, D.H. Crider et al., Low-frequency plasma oscillations at Mars during the October 2003 solar storm. J. Geophys. Res. **110**, A09S33 (2005)
X. Fang, M.W. Liehmohn, A.F. Nagy et al., Escape probability of martian atmospheric ions: controlling effects of the electromagnetic fields. J. Geophys. Res. **115**, A04308 (2010). doi:10.1029/2009JA014929
J.M. Forbes, A.F.C. Bridger, S.W. Bougher et al., Nonmigrating tides in the thermosphere of Mars. J. Geophys. Res. **107**(E11), 5113 (2002). doi:10.1029/2001JE001582
J.L. Fox, Response of the martian thermosphere/ionosphere to enhanced fluxes of solar soft X rays. J. Geophys. Res. **109**, A11310 (2004). doi:10.1029/2004JA010380
J.L. Fox, A.B. Haç, The escape of o from Mars: sensitivity to the elastic cross sections. Icarus **228**, 375 (2014)
D.C. Fritts, S.L. Vadas, K. Wan, J.A. Werne, Mean and variable forcing of the middle atmosphere by gravity waves. J. Atmos. Sol.-Terr. Phys. **68**, 247–265 (2006)
D. Gurnett, D. Kirchner, R. Huff et al., Radar sounding of the ionosphere of Mars. Science **310**, 1929–1933 (2005). doi:10.1126/science.1121868
J.S. Halekas, D.A. Brain, J.P. Eastwood, Large-amplitude compressive 'sawtooth' magnetic field oscillations in the martian magnetosphere. J. Geophys. Res. **116**, A07222 (2011). doi:10.1029/2011JA016590
W. Hanson, G.P. Mantas, Viking electron temperature measurements—evidence for a magnetic field in the martian ionosphere. J. Geophys. Res. **93**, 7538–7544 (1988)
W.B. Hanson, S. Santani, D.R. Zaccaro, The martian ionosphere as observed by the Viking retarding potential analyzers. J. Geophys. Res. **82**, 4351–4363 (1977)
D.S. Harned, Quasineutral hybrid simulation of macroscopic plasma phenomena. J. Comp. Physiol. **47**, 452–462 (1982)
E.M. Harnett, R.M. Winglee, Three-dimensional multifluid simulations of ionospheric loss at Mars from nominal solar wind conditions to magnetic cloud events. J. Geophys. Res. **111**, A09213 (2006). doi:10.1029/2006JA011724
D.E. Huddleston, A.D. Johnstone, Relationship between wave energy and free energy from pickup ions in the comet Halley environment. J. Geophys. Res. **97**, 12217 (1992)
D.E. Huddleston, R.J. Strangeway, X. Blanco-Canoet et al., Io-Jupiter interaction: waves generated by pickup ions. Adv. Space Res. **26**, 1513 (2000)
V. Krasnopolsky, Mars' upper atmosphere and ionosphere at low, medium, and high solar activities: implications for evolution of water. J. Geophys. Res. **107**, 5128–5139 (2002)
W.M. Kaula, *Theory of Satellite Geodesy* (Blaisdell, Waltham, 1966)
A.S. Konopliv, S.W. Asmar, W.M. Folkner et al., Mars high resolution gravity fields from MRO, Mars seasonal gravity, and other dynamical parameters. Icarus **211**, 401–428 (2011)
H. Lammer, Yu.N. Kulikov, H.I.M. Lichtenegger, Thermospheric X-ray and EUV heating by the young Sun on early Venus and Mars. Space Sci. Rev. **122**(1–4), 189–196 (2006)
J.S. Leisner, C.T. Russell, M.K. Dougherty et al., Ion cyclotron waves in Saturn's E ring: initial Cassini observations. Geophys. Res. Lett. **33**, L11101 (2006)
Y. Lee, M.R. Combi, V. Tenishev, S.W. Bougher, Hot carbon corona in Mars' upper thermosphere and exosphere: 1. Mechanisms and structure of the hot corona for low solar activity at equinox. J. Geophys. Res. (2014, submitted)
L. Li, Y. Zhang, Model investigation of the influence of the crustal magnetic field on the oxygen ion distribution in the near martian tail. J. Geophys. Res. **114**, A06215 (2009). doi:10.1029/2008JA013850
L. Li, Y. Zhang, Y. Feng, X. Fang, Y. Ma, Oxygen ion precipitation in the martian atmosphere and its relation with the crustal magnetic fields. J. Geophys. Res. **116**, A08204 (2011). doi:10.1029/2010JA016249
M.W. Liehmohn, R.A. Frahm, J.D. Winningham et al., Numerical interpretation of high–altitude photoelectron observations. Icarus **182**, 383 (2006)
M.W. Liemohn, Y. Ma, A.F. Nagy et al., Numerical modeling of the magnetic topology near Mars auroral observations. Geophys. Res. Lett. **34**, L24202 (2007). doi:10.1029/2007GL031806

R. Lundin, Ion acceleration and outflow from Mars and Venus: an overview. Space Sci. Rev. **162**, 309–334 (2011). doi:10.1007/s11214-011-9811-y

R. Lundin, S. Barabash, M. Holmstrom et al., Atmospheric origin of cold ion escape from Mars. Geophys. Res. Lett. **36**, L17202 (2009). doi:10.1029/2009GL039341

Y.-J. Ma, A.F. Nagy, Ion escape fluxes from Mars. Geophys. Res. Lett. **34**, L08201 (2007). doi:10.1029/2006GL029208

Y.-J. Ma, A.F. Nagy, K.C. Hansen et al., Three-dimensional multispecies MHD studies of the solar wind interaction with Mars in the presence of crustal fields. J. Geophys. Res. **107**(A10), 1282 (2002). doi:10.1029/2002JA009293

Y. Ma, A.F. Nagy, I.V. Sokolov, K.C. Hansen, Three-dimensional, multispecies, high spatial resolution MHD studies of the solar wind interaction with Mars. J. Geophys. Res. **109**, A07211 (2004). doi:10.1029/2003JA010367

Y.J. Ma, C.T. Russell, A.F. Nagy et al., The importance of thermal electron heating in Titan's ionosphere: comparison with Cassini T34 flyby. J. Geophys. Res. **116**, A10213 (2011). doi:10.1029/2011JA016657

C.V. Manning, Y.J. Ma, D.A. Brain et al., Parametric analysis of modeled ion escape from Mars. Icarus **212**(1), 131 (2011)

Y. Matsumoto, K. Seki, Formation of a broad plasma turbulent layer by forward and inverse energy cascades of the Kelvin–Helmholtz instability. J. Geophys. Res. **115**, A10231 (2010). doi:10.1029/009JA014637

M. Matta, P. Withers, M. Mendillo, The composition of Mars' topside ionosphere: effects of hydrogen. J. Geophys. Res. **118**, 2681–2693 (2013). doi:10.1002/jgra.50104

J.C. Marty, G. Balmino, J. Duron et al., Martian gravity field model and its time variations from MGS and ODYSSEY data. Planet. Space Sci. **57**(3), 350–363 (2009)

E. Mazarico, M.T. Zuber, F.G. Lemoine, D.E. Smith, Observation of atmospheric tides in the martian exosphere using Mars reconnaissance Orbiter radio tracking data. Geophys. Res. Lett. **35**, L09202 (2008). doi:10.1029/2008GL033388

A. Määttänen, K. Pérot, F. Montmessin, A. Hauchecorne, Mesospheric clouds on Mars and on Earth, in *Comparative Climatology of Terrestrial Planets*, ed. by S.J. Mackwell et al. (Univ. of Arizona, Tucson, 2013), pp. 393–413. doi:10.2458/azu_uapress_9780816530595-chi6

T.H. McConnoochie, J.F. Bell, M. Savransky et al., THEMIS_VIS observations of clouds in the martian mesosphere: altitudes, wind speeds, and decameter-scale morphology. Icarus **210**, 545–565 (2010). doi:10.1016/j.icarus.2010.07.021

A.S. Medvedev, E. Yiğit, Thermal effects of internal gravity waves in the martian upper atmosphere. Geophys. Res. Lett. **39**, L05201 (2012). doi:10.1029/2012GL050852

A.S. Medvedev, E. Yigit, P. Hartogh, E. Becker, Influence of gravity waves on the martian atmosphere: general circulation modeling. J. Geophys. Res. **116**, E10004 (2011). doi:10.1029/2011JE003848

M. Mendillo, A. Lollo, P. Withers et al., Modeling mars' ionosphere with constraints from same-day observations by Mars Global Surveyor and Mars Express. J. Geophys. Res. **116**, A11303 (2011). doi:10.1029/2011JA016865

M. Mendillo, A. Marusiak, P. Withers et al., A new semiempirical model of the peak electron density of the Martian ionosphere. Geophys. Res. Lett. **40**, 5363–5365 (2013a). doi:10.1002/2013GL05763

M. Mendillo, C. Narvaez, P. Withers et al., Variability in ionospheric total electron content at Mars. Planet. Space Sci. **86**, 117–129 (2013b)

D.L. Mitchell, C. Lin, H. Mazelle et al., Probing Mars' crustal magnetic field and ionosphere with the MGS Electron Reflectometer. J. Geophys. Res. **106**(E10), 23419–23427 (2001). doi:10.1029/2000JE001435

F. Montmessin, J.-L. Bertaux, O. Korablev et al., Subvisible CO_2 ice clouds detected in the mesosphere of Mars. Icarus **183**, 403–410 (2006). doi:10.1016/j.icarus.2006.03.015

F. Montmessin, B. Gondet, J. Bibring et al., Hyperspectral imaging of convective CO_2 ice clouds in the equatorial mesosphere of Mars. J. Geophys. Res. **112**, E11S90 (2007). doi:10.1029/2007JE002944

D.H. Morgan, D.A. Gurnett, D.L. Kirchner et al., Variation of the martian ionospheric electron density from Mars Express radar soundings. J. Geophys. Res. **113**, A09303 (2008). doi:10.1029/2008JA013313

A.F. Nagy, T.E. Cravens, Hot oxygen atoms in the upper atmosphere of Venus and Mars. Geophys. Res. Lett. **15**, 433 (1988)

A.F. Nagy, M. Liemohn, J.L. Fox, J. Kim, Hot carbon densities in the exosphere of Mars. J. Geophys. Res. **106**, 21565 (2001)

D. Najib, A.F. Nagy, G. Tóth, Y. Ma, Three-dimensional, multifluid, high spatial resolution MHD model studies of the solar wind interaction with Mars. J. Geophys. Res. **116**, A05204 (2011)

A.O. Nier, M.B. McElroy, Composition and structure of Mars' upper atmosphere: results from the Neutral Mass Spectrometers on Viking 1 and 2. J. Geophys. Res. **82**, 4341–4349 (1977)

T. Penz, N.V. Erkaev, H.K. Biernat et al., Ion loss on Mars caused by the Kelvin–Helmholtz instability. Planet. Space Sci. **52**, 1157–1167 (2004). doi:10.1016/j.pss.2004.06.001

G. Picardi, J.J. Plaut, D. Biccari et al., Radar soundings of the subsurface of Mars. Science **310**(5756), 1925–1928 (2005). doi:10.1126/science.1122165

K.G. Powell, P.L. Roe, T.J. Linde et al., A solution-adaptive upwind scheme for ideal magnetohydrodynamics. J. Comput. Phys. **154**, 284 (1999)

P. Rosenblatt, V. Lainey, S. Le Maistre et al., Accurate Mars Express orbits to improve the determination of the mass and ephemeris of the martian moons. Planet. Space Sci. **56**, 1043–1053 (2008)

P. Rosenblatt, S.L. Bruinsma, I.C.F. Müller-Wodarg et al., First ever in situ observations of Venus' polar upper atmosphere density using the tracking data of the Venus eXpress Atmospheric Drag Experiment (VExADE). Icarus, Special Issue: Advances in Venus Science **217**(2), 831–838 (2012)

R. Schunk, A.F. Nagy, *Ionospheres* (Cambridge University Press, Cambridge, 2009)

H. Shinagawa, T. Cravens, The ionospheric effects of a weak intrinsic magnetic field at Mars. J. Geophys. Res. **97**, 1027–1035 (1992)

B.D. Shizgal, G.G. Arkos, Nonthermal escape of the atmospheres of Venus, Earth, and Mars. Rev. Geophys. **34**, 483–505 (1996). doi:10.1029/96RG02213

D.E. Siskind, D.R. Marsh, M.G. Mlynczak et al., Decreases in atomic hydrogen over the summer pole: evidence for dehydration from polar mesospheric clouds? Geophys. Res. Lett. **35**, L13809 (2008). doi:10.1029/2008GL033742

A. Spiga, F. Gonzalez-Galindo, M.-A. Lopez-Valverde, F. Forget, Gravity waves, cold pockets and CO_2 clouds in the martian mesosphere. Geophys. Res. Lett. **39**, L02201 (2012). doi:10.1029/2011GL050343

M.H. Stevens, D.E. Siskind, S.D. Eckermann et al., Tidally induced variations of polar mesospheric cloud altitudes and ice water content using a data assimilation system. J. Geophys. Res. **115**, D18209 (2010). doi:10.1029/2009JD013225

D.W. Swift, Use of a hybrid code to model the Earth's magnetosphere. Geophys. Res. Lett. **22**, 311 (1995)

N. Terada, S. Machida, H. Shinagawa, Global hybrid simulation of the Kelvin–Helmholtz instability at the Venus ionopause. J. Geophys. Res. **107**, 11471 (2002). doi:10.1029/2001JA009224

N. Terada, Y.N. Kulikov, H. Lammer et al., Atmosphere and water loss from early Mars under extreme solar wind and EUV conditions. Astrobiology **9**, 55–70 (2009b). doi:10.1089/ast.2008.0250

N. Terada, H. Shinagawa, T. Tanaka et al., A three-dimensional, multi-species, comprehensive MHD model of the solar wind interaction with the planet Venus. J. Geophys. Res. **114**, A09208 (2009a). doi:10.1029/2008JA013937

K. Terada et al., A paper in preparation on DCSM simulation of Mars atmosphere and exosphere (2014)

R.L. Tokar, R.J. Wilson, R.E. Johnson et al., Cassini detection of water-group pick-up ions in the Enceladus torus. Geophys. Res. Lett. **33**, L14202 (2008)

G. Toth, I.V. Sokolov, T.I. Gombosi et al., Space weather modeling framework: a new tool for the space science community. J. Geophys. Res. **110**, A12226 (2005). doi:10.1029/2005JA011126

G. Toth, B. Vander Holst, I.V. Sokolov et al., Adaptive numerical algorithms in space weather modeling. J. Comput. Phys. **231**(3), 870–903 (2012). doi:10.1016/j.jcp.2011.02.006

A. Valeille, V. Tenishev, S.W. Bougher et al., Three-dimensional study of Mars upper thermosphere/ionosphere and hot oxygen corona: 1. General description and results at equinox for solar low conditions. J. Geophys. Res. **114**, E11005 (2009a)

A. Valeille, M.R. Combi, S.W. Bougher et al., Three-dimensional study of Mars upper thermosphere/ionosphere and hot oxygen corona: 2. Solar cycle, seasonal variations, and evolution over history. J. Geophys. Res. **114**, E11006 (2009b)

A. Valeille, M.R. Combi, V. Tenishev et al., A study of suprathermal oxygen atoms in Mars upper thermosphere and exosphere over the range of limiting conditions. Icarus **206**, 18 (2010a)

A. Valeille, M.R. Combi, V. Tenishev et al., Water loss and evolution of the upper atmosphere and exosphere over martian history. Icarus **206**, 28 (2010b)

M. Vincendon, C. Pilorget, B. Gondetet et al., Observations of mesospheric CO_2 and H_2O clouds on Mars. J. Geophys. Res. **116**, E00J02 (2011). doi:10.1029/2011JE003827

P. Withers, A review of observed variability in the dayside ionosphere of Mars. Adv. Space Res. **44**, 277–307 (2009). doi:10.1016/J.asr.2009.04.027

P. Withers, K. Fallows, Z. Girazian et al., A clear view of the multifaceted dayside ionosphere of Mars. Geophys. Res. Lett. **39**, L18202 (2012). doi:10.1029/2012GL053193

M. Yagi, F. Leblanc, J.Y. Chaufray, F. Gonzalez-Galindo et al., Mars exospheric thermal and non-thermal components: seasonal and local variations. Icarus **221**, 682–693 (2012)

M. Yamauchi et al., IMF direction derived from cycloid-like ion distributions observed by Mars Express. Space Sci. Rev. **126**, 239 (2006)